

Parity-violating neutron spin rotation in hydrogen and deuterium

Harald W. Griesshammer,^{1,*} Matthias R. Schindler,^{1,2,†} and Roxanne P. Springer^{3,‡}

¹*Institute for Nuclear Studies, Department of Physics,*

The George Washington University, Washington DC 20052, USA

²*Department of Physics and Astronomy,*

University of South Carolina, Columbia, SC 29208, USA

³*Department of Physics, Duke University, Durham, NC 27708, USA*

(Dated: 26th September 2011)

We calculate the (parity-violating) spin rotation angle of a polarized neutron beam through hydrogen and deuterium targets, using pionless effective field theory up to next-to-leading order. Our result is part of a program to obtain the five leading independent low-energy parameters that characterize hadronic parity-violation from few-body observables in one systematic and consistent framework. The two spin-rotation angles provide independent constraints on these parameters. Our result for np spin rotation is $\frac{1}{\rho} \frac{d\phi_{PV}^{np}}{dt} = [4.5 \pm 0.5] \text{ rad MeV}^{-\frac{1}{2}} \left(2g^{(3S_1-3P_1)} + g^{(3S_1-1P_1)} \right) - [18.5 \pm 1.9] \text{ rad MeV}^{-\frac{1}{2}} \left(g_{(\Delta I=0)}^{(1S_0-3P_0)} - 2g_{(\Delta I=2)}^{(1S_0-3P_0)} \right)$, while for nd spin rotation we obtain $\frac{1}{\rho} \frac{d\phi_{PV}^{nd}}{dt} = [8.0 \pm 0.8] \text{ rad MeV}^{-\frac{1}{2}} g^{(3S_1-1P_1)} + [17.0 \pm 1.7] \text{ rad MeV}^{-\frac{1}{2}} g^{(3S_1-3P_1)} + [2.3 \pm 0.5] \text{ rad MeV}^{-\frac{1}{2}} \left(3g_{(\Delta I=0)}^{(1S_0-3P_0)} - 2g_{(\Delta I=1)}^{(1S_0-3P_0)} \right)$, where the $g^{(X-Y)}$, in units of $\text{MeV}^{-\frac{3}{2}}$, are the presently unknown parameters in the leading-order parity-violating Lagrangian. Using naïve dimensional analysis to estimate the typical size of the couplings, we expect the signal for standard target densities to be $\left| \frac{d\phi_{PV}}{dt} \right| \approx [10^{-7} \dots 10^{-6}] \frac{\text{rad}}{\text{m}}$ for both hydrogen and deuterium targets. We find no indication that the nd observable is enhanced compared to the np one. All results are properly renormalized. An estimate of the numerical and systematic uncertainties of our calculations indicates excellent convergence. An appendix contains the relevant partial-wave projectors of the three-nucleon system.

*Electronic address: hgrie@gwu.edu

†Electronic address: schindler@sc.edu

‡Electronic address: rps@phy.duke.edu

I. INTRODUCTION

Parity-violating nucleon-nucleon interactions cause the spin of transversely polarized neutrons to undergo a rotation when traveling through a target medium, even in the absence of magnetic fields. In this paper we report the results of a calculation of neutron spin rotation from neutron-proton and neutron-deuteron forward scattering using pionless effective field theory, EFT($\not{\pi}$). This work is part of an effort to provide one consistent EFT($\not{\pi}$) framework with reliable theoretical uncertainties to parity-violating (PV) interactions in few-nucleon systems. We hope that the results presented here, along with the results from Refs. [1, 2], will assist in the planning, analysis, and interpretation of related PV experiments.

The PV component of the force between nucleons stems from the weak interactions between the standard model constituents of the nucleons. Compared to the parity-conserving (PC) part, it is typically suppressed by a factor of $\sim 10^{-7}$ to 10^{-6} ; for reviews see e.g. Refs. [3, 4]. Parity-violating neutron spin rotation observables were first discussed by Michel in 1964 [5] and studied further in Refs. [6–8]. Recently, an upper bound on the effect in Helium-4 was obtained at NIST [9].

At present, the effects of hadronic parity violation on the nuclear level cannot be predicted from first principles. Early approaches to PV nucleon-nucleon (NN) interactions include the parameterization in terms of S-P wave transitions [10] and the more widely used phenomenological meson-exchange models, particularly the framework developed by Desplanques, Donoghue and Holstein (DDH) in Ref. [11]. The DDH approach provides estimated ranges for PV meson-nucleon couplings based on a number of model assumptions. Using the “best values,” it has been applied to the study of neutron spin rotation on various targets [12–15]. Calculations have also been performed in the so-called hybrid formalism [15–17], where phenomenological wave functions in the strong sector are combined with a PV effective field theory (EFT) treatment. We discuss this further in Sec. VII.

In order to avoid model assumptions and to treat all interactions within a unified framework, we apply effective field theory techniques consistently to the neutron-hydrogen and neutron-deuterium systems. The identification of a small parameter allows a systematic expansion of our results and a reliable estimate of the size of theoretical errors. In particular, since typical neutron energies in parity-violating spin-rotation experiments on the lightest nuclei are low enough that pion exchange cannot be resolved, we use the pionless EFT with

only nucleons as dynamical degrees of freedom. This theory has proven highly successful in the parity-conserving sector; for an overview see e.g. Refs. [18–20]. For early EFT descriptions of hadronic parity violation see Refs. [21–23]. A comprehensive formulation of PV effects in EFTs with and without pions was given in Ref. [24].

In the PV sector of EFT(π), five independent operators appear at leading order (LO) in EFT(π). They correspond to the five transition amplitudes from Ref. [10] expressed in a field theory language. The five accompanying parameters, or low-energy constants (LECs), encode the unresolved short-distance physics. At present, only experimental input can determine these couplings without introducing additional model dependence. Note, however, that for the pionful sector a first study using lattice simulations to determine the PV πNN coupling has been performed [25]. Our final, next-to-leading order (NLO) results for np and nd spin rotation provide these processes in terms of the PV LECs, along with estimates of the associated theoretical errors. Measurements of these observables can determine two independent combinations of the PV low-energy constants.

This article is organized as follows: We first review the general formalism of neutron spin rotation in Sec. II and present the necessary PC and PV pieces of the Lagrangian in Secs. III and IV, respectively. The results for neutron spin-rotation on the proton up to NLO, along with error estimates, are given in Sec. V. The results for deuterium up to NLO are derived with a detailed discussion of the expected theoretical uncertainties in Sec. VI. In Sec. VII we estimate numerical predictions and compare with earlier work. Conclusions and outlook are given in Sec. VIII. Appendices contain the general construction principle for the partial-wave projectors of the three-nucleon system and its results for the S- and P-waves as well as details of the numerical calculations.¹

II. NEUTRON SPIN ROTATION – GENERAL FORMALISM

In this section, we define the spin rotation angle, its relation to the scattering amplitude, and the associated conventions we will use. Important resources are Refs.[5–8, 27], but note that conventions vary.

A beam of very-low energy neutrons passing through a medium picks up a phase factor

¹ After completion of this article a paper appeared by Vanasse [26], with an analysis of neutron spin rotation off the deuteron using pionless EFT to leading order.

from scattering in the target. This phase factor is related to the index of refraction n of the medium. In the simplest case of very low-energy scattering with plane waves describing the incoming state, the phase accumulated after traversing a target of thickness l is given by

$$\varphi = \text{Re}(n - 1)k_{\text{lab}}l, \quad (\text{II.1})$$

where k_{lab} is the magnitude of the wave vector of the incoming particle. The index of refraction is in turn related to the scattering length a by

$$n - 1 = -\frac{2\pi\rho a}{k_{\text{lab}}^2}, \quad (\text{II.2})$$

where ρ is the density of scattering centers in the target. In our convention, the scattering length and scattering amplitude at zero energy are related by

$$\mathcal{M} = -\frac{2\pi}{\mu}a, \quad (\text{II.3})$$

with μ the reduced mass of the beam-target system. The phase φ can therefore be written as

$$\varphi = \rho l \frac{\mu}{k_{\text{lab}}} \text{Re}(\mathcal{M}). \quad (\text{II.4})$$

For a beam chosen in the $+z$ direction, a perpendicular polarization in the $+x$ direction can be written as

$$|x_+\rangle = \frac{1}{\sqrt{2}}(|+\rangle + |-\rangle), \quad (\text{II.5})$$

where the states $|\pm\rangle$ represent states with positive/negative helicity along $+\hat{z}$. When traversing a medium, each helicity state evolves with a phase factor:

$$\frac{1}{\sqrt{2}}(e^{-i\phi_+}|+\rangle + e^{-i\phi_-}|-\rangle) = \frac{1}{\sqrt{2}}e^{-i\phi_+}(|+\rangle + e^{i(\phi_+ - \phi_-)}|-\rangle). \quad (\text{II.6})$$

As long as $\phi_+ = \phi_-$, which is the case for parity-conserving interactions, the polarization of the beam is unchanged; the state simply picks up an overall phase factor. In the case of parity violation, however, $\phi_+ \neq \phi_-$ and the neutron spin is rotated by an amount

$$\phi_{\text{PV}} = \phi_+ - \phi_-. \quad (\text{II.7})$$

A positive value of the spin rotation angle ϕ_{PV} corresponds to a rotation about the neutron momentum in the sense of a right-handed screw. Using Eq. (II.4), the spin rotation angle per unit length l is

$$\frac{1}{\rho} \frac{d\phi_{\text{PV}}}{dl} = \frac{\mu}{k_{\text{lab}}} \text{Re}(\mathcal{M}_+ - \mathcal{M}_-), \quad (\text{II.8})$$

where \mathcal{M}_{\pm} is the scattering amplitude for \pm -helicity neutrons including the statistical mixture of available target spins. For further details see Refs. [6, 8].

III. PARITY-CONSERVING LAGRANGIANS AND AMPLITUDES

A. Two-Nucleon Sector

A description of EFT(π) and its power counting can be found in Refs. [18–20], for example. Pionless EFT is applicable to energies $E < m_\pi^2/M$, where m_π and M are the pion and nucleon mass, respectively. The short-distance details of the interactions are encoded in the low-energy couplings (LECs) of NN contact interactions. Operators and observables are organized in terms of the small dimensionless expansion parameter $Q = \frac{p_{\text{typ}}}{\Lambda_\pi}$, where p_{typ} is the typical external momentum or momentum transfer and $\Lambda_\pi \sim m_\pi$ is the breakdown scale of the theory (the scale at which pion exchange can be resolved). The expansion parameter is typically 1/5 to 1/3. The following leading-order (LO) and next-to-leading order (NLO) calculations only require S-wave interactions in the parity-conserving NN sector; higher partial waves are suppressed according to the power counting. It is convenient (in particular for three-body calculations) to introduce spin-triplet and spin-singlet dibaryon fields d_t and d_s with the quantum numbers of the corresponding two-nucleon S-wave states [28–30]. The dibaryon (auxiliary) field d_t also serves as the deuteron interpolating field since both have identical quantum numbers. The relevant terms of the Lagrangian up to NLO are

$$\begin{aligned} \mathcal{L}_{PC} = & N^\dagger \left(i\partial_0 + \frac{\vec{\partial}^2}{2M} \right) N - y \left[d_t^{i\dagger} (N^T P_t^i N) + \text{H.c.} \right] - y \left[d_s^{A\dagger} (N^T P_s^A N) + \text{H.c.} \right] \\ & + d_t^{i\dagger} \left[\Delta_t - c_{0t} \left(i\partial_0 + \frac{\vec{\partial}^2}{4M} + \frac{\gamma_t^2}{M} \right) \right] d_t^i + d_s^{A\dagger} \left[\Delta_s - c_{0s} \left(i\partial_0 + \frac{\vec{\partial}^2}{4M} + \frac{\gamma_s^2}{M} \right) \right] d_s^A \\ & + \dots, \end{aligned} \quad (\text{III.1})$$

using the conventions of Ref. [31]. $N = \begin{pmatrix} p \\ n \end{pmatrix}$ is the isospin doublet of nucleon Weyl spinors p (proton) and n (neutron). With σ_i (τ_A) the Pauli matrices in spin (isospin) space, the matrices $P_t^i = \frac{1}{\sqrt{8}}\tau_2\sigma_2\sigma_i$ and $P_s^A = \frac{1}{\sqrt{8}}\tau_2\tau_A\sigma_2$ project two-nucleon states onto the $^3\text{S}_1$ and $^1\text{S}_0$ partial waves [32].

The parameters of the Lagrangian are fixed using Z-parameterization [31, 33]. Choosing

$$y^2 = \frac{4\pi}{M} \quad , \quad (\text{III.2})$$

the LO parameters $\Delta_{s/t}$ are determined from the poles of the NN S-wave scattering amplitudes at $i\gamma_{s/t}$. In the $^3\text{S}_1$ -wave, this reproduces the experimental binding energy of the

deuteron $B_d = -\gamma_t^2/M$. The leading-order dibaryon propagators are then given by

$$D_{s/t}^{\text{LO}}(q_0, \vec{q}) = \frac{1}{\gamma_{s/t} - \sqrt{\frac{q^2}{4} - Mq_0 - i\epsilon}} . \quad (\text{III.3})$$

At NLO, only the additional parameters $c_{0s/t}$ enter. In Z -parameterization, they are chosen such that the residues of the poles in the dibaryon propagators do not receive any corrections beyond NLO; see again Ref. [31] for details:

$$c_{0s/t} = -\frac{M}{2\gamma_{s/t}} (Z_{s/t} - 1) , \quad (\text{III.4})$$

where $Z_{s/t} = 1/(1 - \gamma_{s/t}\rho_{s/t})$ is related to the effective range $\rho_{s/t}$. Up to NLO, the dibaryon propagators in Eq. (III.3) are modified by an insertion of the effective-range term $c_{0s/t}$ of the Lagrangian of Eq. (III.1):

$$D_{s/t}^{\text{LO+NLO}}(q_0, \vec{q}) = D_{s/t}^{\text{LO}}(q_0, \vec{q}) + D_{s/t}^{\text{NLO}}(q_0, \vec{q}) , \quad (\text{III.5})$$

with the NLO correction (Z -parameterization variant in the second line)

$$\begin{aligned} D_{s/t}^{\text{NLO}}(q_0, \vec{q}) &= iD_{s/t}^{\text{LO}}(q_0, \vec{q}) (-c_{0s/t}) \left(q_0 - \frac{q^2}{4M} + \frac{\gamma_{s/t}^2}{M} \right) iD_{s/t}^{\text{LO}}(q_0, \vec{q}) \\ &= \frac{\gamma_{s/t} + \sqrt{\frac{q^2}{4} - Mq_0 - i\epsilon}}{\gamma_{s/t} - \sqrt{\frac{q^2}{4} - Mq_0 - i\epsilon}} \frac{Z_{s/t} - 1}{2\gamma_{s/t}} . \end{aligned} \quad (\text{III.6})$$

Calculations with a deuteron as an external state require wave function renormalization, \mathcal{Z}_t . In Z -parameterization, the LO expression is

$$\mathcal{Z}_t^{\text{LO}} = \frac{2\gamma_t}{M} , \quad (\text{III.7})$$

and up to NLO

$$\mathcal{Z}_t^{\text{LO+NLO}} = \frac{2\gamma_t}{M} Z_t = \frac{2\gamma_t}{M} \frac{1}{(1 - \gamma_t\rho_t)} . \quad (\text{III.8})$$

With $Z_t = 1.6908$, the NLO correction results in a 70%-shift from the LO value. While this contribution is much larger than expected from naïve power counting, there are no further corrections to \mathcal{Z}_t at higher orders. This has the important advantage that the correct asymptotic normalization of the deuteron wave function at large distances r is exactly reproduced at NLO, with no corrections at higher orders:

$$\Psi_{\text{deuteron}}(r \rightarrow \infty) = \sqrt{\frac{\gamma_t Z_t}{2\pi}} \frac{e^{-\gamma_t r}}{r} . \quad (\text{III.9})$$

Taking into account the unusually large NLO term therefore significantly increases overall convergence of the expansion of $\text{EFT}(\not{\pi})$, as demonstrated e.g. in Refs. [31, 33].

B. Three-Nucleon Sector

The consistency requirement of including a three-nucleon interaction (3NI) in the $^2S_{\frac{1}{2}}$ channel even at LO is discussed in reviews; see e.g. Refs. [18–20]. The corresponding Lagrangian is given by

$$\mathcal{L}_{3N} = \frac{y^2 M H_0(\Lambda)}{3\Lambda^2} [d_t^i(\sigma_i N) - d_s^A(\tau_A N)]^\dagger [d_t^i(\sigma_i N) - d_s^A(\tau_A N)], \quad (\text{III.10})$$

where $H_0(\Lambda)$ denotes the three-nucleon coupling, which depends on the UV regulator Λ . This is the only parameter of Nd scattering up to NLO not determined from NN experiments. The 3NI strength $H_0(\Lambda)$ can be chosen to reproduce the triton binding energy, or the $^2S_{\frac{1}{2}}$ -scattering length. Choosing different low-energy data to fix it provides one method to estimate the theoretical uncertainties in Sec. VI E.

The parity-conserving nd scattering amplitude is found by solving a Faddeev equation, see e.g. Ref. [31]. Its pictorial representation in Fig. 1 specifies the center-of-mass kinematics: The total non-relativistic energy is E , and the momentum of the incoming (outgoing) deuteron is \vec{k} (\vec{p}). The on-shell point is at $E = \frac{3\vec{k}^2}{4M} - \frac{\gamma_t^2}{M} + i\epsilon$ and $p = k$.

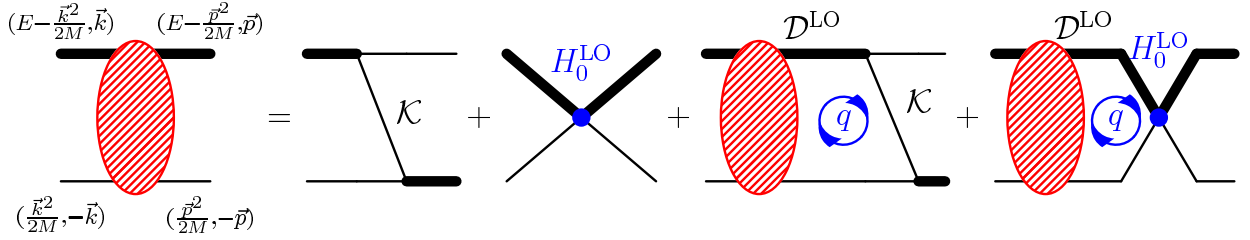


Figure 1: Nucleon-deuteron scattering at LO. Shaded ellipse: LO amplitude t^{LO} ; thick line: LO dibaryon propagator \mathcal{D}^{LO} of Eq. (III.12); thin line (\mathcal{K}): propagator of the exchanged nucleon; disc: PC 3NI (H_0^{LO}).

In the dibaryon framework, the three-nucleon system receives contributions from Nd_s and Nd_t configurations, which are conveniently taken into account by decomposing all operators and amplitudes into the so-called cluster-decomposition basis (see Ref. [31, App. A.1] and our App. A),

$$\mathcal{O} = N_{b\beta}^\dagger \begin{pmatrix} d_{t,j}^\dagger & d_{s,B}^\dagger \end{pmatrix} \begin{pmatrix} \mathcal{O}(Nd_t \rightarrow Nd_t)_i^j & \mathcal{O}(Nd_s \rightarrow Nd_t)_A^j \\ \mathcal{O}(Nd_t \rightarrow Nd_s)_i^B & \mathcal{O}(Nd_s \rightarrow Nd_s)_A^B \end{pmatrix}^{b\beta}_{a\alpha} \begin{pmatrix} d_t^i \\ d_s^A \end{pmatrix} N^{a\alpha}, \quad (\text{III.11})$$

where the spinor and isospinor indices (α, β) and (a, b) , respectively, are often suppressed in the following. The vector indices $i, j = (1, 2, 3)$ label the spin Pauli matrices while $A, B = (1, 2, 3)$ label the isospin Pauli matrices. As an example, the LO dibaryon propagator in the cluster-decomposition basis is defined by a diagonal matrix in terms of the dibaryon propagators Eq. (III.3):

$$\mathcal{D}^{\text{LO}}(q_0, \vec{q}) = \begin{pmatrix} D_t^{\text{LO}}(q_0, \vec{q}) & 0 \\ 0 & D_s^{\text{LO}}(q_0, \vec{q}) \end{pmatrix}. \quad (\text{III.12})$$

An analogous expression holds for the NLO correction of Eq. (III.6).

The spin-quartet channel only receives contributions from $Nd_t \rightarrow Nd_t$, and the corresponding amplitude t_q is the solution to an integral equation that only involves the (11)-element of the cluster matrix (the argument $(E; p_{\text{in}}, p_{\text{out}})$ applies to each entry in the matrix):

$$\begin{pmatrix} t_q^{(L)} & 0 \\ 0 & 0 \end{pmatrix} (E; k, p) = -4\pi \mathcal{K}^{(L)}(E; k, p) \begin{pmatrix} 1 & 0 \\ 0 & 0 \end{pmatrix} \\ + \frac{2}{\pi} \int_0^\Lambda dq q^2 \mathcal{K}^{(L)}(E; q, p) \begin{pmatrix} 1 & 0 \\ 0 & 0 \end{pmatrix} \mathcal{D}^{\text{LO}}(E; q) \begin{pmatrix} t_q^{(L)} & 0 \\ 0 & 0 \end{pmatrix} (E; k, q), \quad (\text{III.13})$$

with Λ the UV regulator. The projection of the exchange-nucleon propagator onto a specific orbital angular momentum L is

$$\mathcal{K}^{(L)}(E; q, p) = \frac{1}{2} \int_{-1}^1 d \cos \theta \frac{P_L(\cos \theta)}{p^2 + q^2 - ME + pq \cos \theta} = \frac{(-1)^L}{pq} Q_L \left(\frac{p^2 + q^2 - ME}{pq} \right), \quad (\text{III.14})$$

with $P_L(z)$ and $Q_L(z)$ the L th Legendre polynomials of the first and second kind with complex argument, respectively [34], and $\theta = \angle(\vec{p}; \vec{q})$.

In the spin-doublet channel, amplitudes with different cluster-decompositions mix, so

that with $t_{d,xy}^{(L)}$ denoting the amplitude for the process $Nd_x \rightarrow Nd_y$ and $x, y \in \{s, t\}$:

$$\begin{aligned} \begin{pmatrix} t_{d,tt}^{(L)} & t_{d,st}^{(L)} \\ t_{d,ts}^{(L)} & t_{d,ss}^{(L)} \end{pmatrix} (E; k, p) = 2\pi \left[\mathcal{K}^{(L)}(E; k, p) \begin{pmatrix} 1 & -3 \\ -3 & 1 \end{pmatrix} + \delta_0^L \frac{2H_0(\Lambda)}{\Lambda^2} \begin{pmatrix} 1 & -1 \\ -1 & 1 \end{pmatrix} \right] \\ - \frac{1}{\pi} \int_0^\Lambda dq q^2 \left[\mathcal{K}^{(L)}(E; q, p) \begin{pmatrix} 1 & -3 \\ -3 & 1 \end{pmatrix} + \delta_0^L \frac{2H_0(\Lambda)}{\Lambda^2} \begin{pmatrix} 1 & -1 \\ -1 & 1 \end{pmatrix} \right] \\ \times \mathcal{D}^{\text{LO}}(E; q) \begin{pmatrix} t_{d,tt}^{(L)} & t_{d,st}^{(L)} \\ t_{d,ts}^{(L)} & t_{d,ss}^{(L)} \end{pmatrix} (E; k, q) . \end{aligned} \quad (\text{III.15})$$

Since there is no partial-wave mixing in the PC sector even at NLO, the quartet- and doublet scattering amplitudes can be combined into one cluster matrix

$$t^{\text{LO}}[{}^{2S+1}L_J; k, q] = \begin{cases} \begin{pmatrix} t_q^{(L)} & 0 \\ 0 & 0 \end{pmatrix} (E; k, q) & \text{for the spin-quartet, } S = \frac{3}{2} \\ \begin{pmatrix} t_{d,tt}^{(L)} & t_{d,st}^{(L)} \\ t_{d,ts}^{(L)} & t_{d,ss}^{(L)} \end{pmatrix} (E; k, q) & \text{for the spin-doublet, } S = \frac{1}{2} \end{cases}, \quad (\text{III.16})$$

where S is the spin, L the orbital angular momentum and J the total angular momentum of the ${}^{2S+1}L_J$ partial wave considered.

For the NLO PC amplitudes, we use the so-called “partially-resummed” formalism, in which the kernel and inhomogeneous part of the integral equations are expanded to NLO and then iterated, see Fig. 2 and Ref. [35]. This modifies the dibaryon propagators in Eqs. (III.13/III.15) by an insertion of the effective-range contribution, i.e. by replacing $\mathcal{D}^{\text{LO}}(E; q)$ with $\mathcal{D}^{\text{LO+NLO}}(E; q)$, see Eq. (III.5). No new PC 3NI enters at NLO, but in order to reproduce the three-nucleon observable, H_0 has to be adjusted at NLO. This is most conveniently achieved by dividing H_0 into a LO piece H_0^{LO} and a term at NLO, H_0^{NLO} . In this approach, in addition to *all* LO and NLO contributions, some higher-order contributions are also included in the amplitude referred to as $t^{\text{LO+NLO}}$. This does not increase the accuracy of the calculations, which is still set by the order to which the kernel is expanded. Figure 3 shows the cutoff dependence of the 3NI H_0 at LO and LO+NLO in the partially-resummed formulation. While H_0 varies considerably, observables are cutoff-independent,

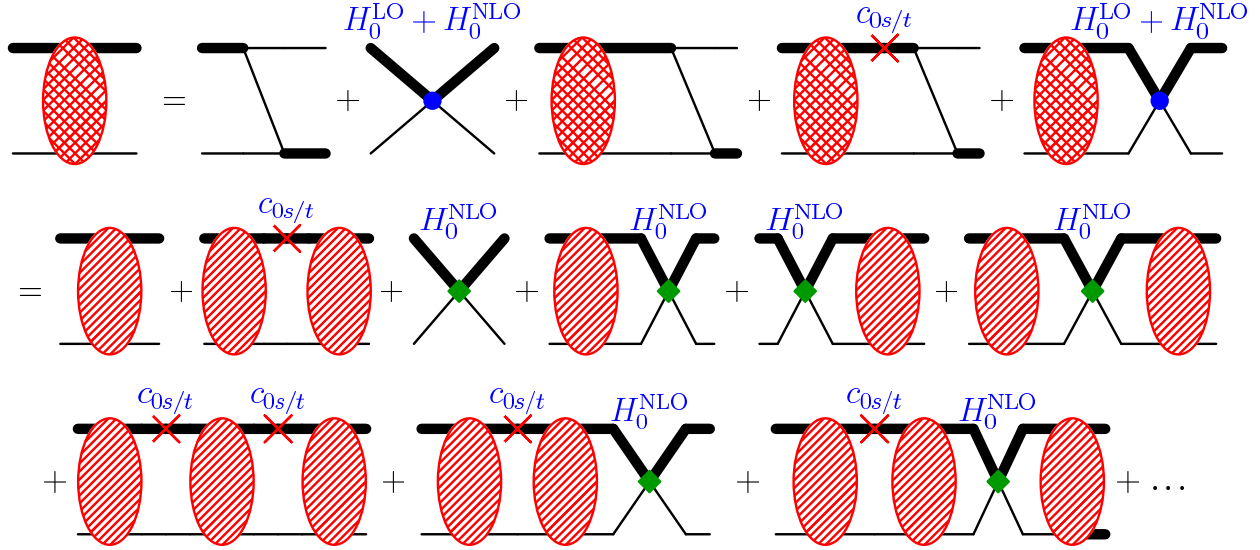


Figure 2: Top row: Nucleon-deuteron scattering in the partially-resummed formalism at NLO. Middle row: all LO and NLO contributions. Bottom row: some of the diagrams which are strictly higher order than NLO but resummed for convenience. Cross-hatched ellipse: $t^{\text{LO+NLO}}$ as defined in the text; cross: insertion of the effective-range correction $c_{0s/t}$ to the dibaryon propagator; diamond: PC 3NI H_0^{NLO} .

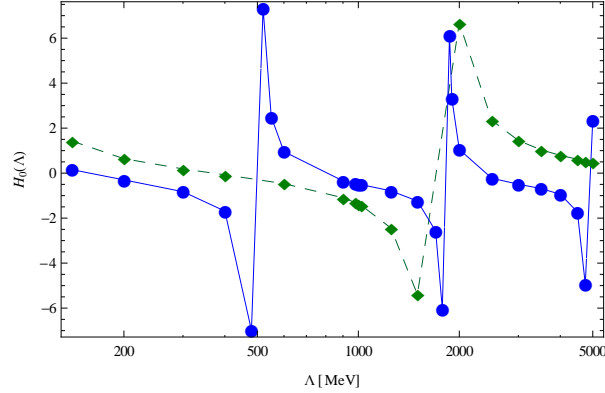


Figure 3: Cutoff dependence of the $^2\text{S}_{1/2}$ -wave PC 3NI $H_0(\Lambda)$, determined to reproduce the $^2\text{S}_{1/2}$ scattering length. \blacklozenge (dashed lines): LO; \bullet (solid lines): LO+NLO in the partially-resummed formulation. The linear extrapolations are only meant to guide the eye.

see e.g. [31]. This point will be of importance in the discussion of renormalization of the PV amplitudes in Secs. VIB, VIC and App. B.

The following parameters are used [31]: $\hbar c = 197.327$ MeV fm, the isospin-averaged nucleon mass $M = 938.918$ MeV; $\gamma_t = 45.7025$ MeV, $\gamma_s = -7.890$ MeV, $Z_t = 1.6908$, and $Z_s = 0.9015$ are the effective-range parameters of the NN system; and the nd ${}^2S_{\frac{1}{2}}$ scattering length $a_3 = 0.65$ fm [36] or triton binding energy $B_3 = 8.48$ MeV determines the 3NI $H_0(\Lambda)$.

IV. PARITY-VIOLATING LAGRANGIAN

The leading-order PV Lagrangian relevant to our calculation is given in terms of five S–P wave transitions [2],

$$\begin{aligned} \mathcal{L}_{PV} = - & \left[g^{(3S_1-1P_1)} d_t^{i\dagger} \left(N^T \sigma_2 \tau_2 i \overleftrightarrow{\partial}_i N \right) \right. \\ & + g_{(\Delta I=0)}^{(1S_0-3P_0)} d_s^{A\dagger} \left(N^T \sigma_2 \vec{\sigma} \cdot \tau_2 \tau_A i \overleftrightarrow{\partial} N \right) \\ & + g_{(\Delta I=1)}^{(1S_0-3P_0)} \epsilon^{3AB} d_s^{A\dagger} \left(N^T \sigma_2 \vec{\sigma} \cdot \tau_2 \tau^B i \overleftrightarrow{\partial} N \right) \\ & + g_{(\Delta I=2)}^{(1S_0-3P_0)} \mathcal{I}^{AB} d_s^{A\dagger} \left(N^T \sigma_2 \vec{\sigma} \cdot \tau_2 \tau^B i \overleftrightarrow{\partial} N \right) \\ & \left. + g^{(3S_1-3P_1)} \epsilon^{ijk} d_t^{i\dagger} \left(N^T \sigma_2 \sigma^k \tau_2 \tau_3 i \overleftrightarrow{\partial}^j N \right) \right] + \text{H.c.} + \dots, \end{aligned} \quad (\text{IV.1})$$

where $a \overleftrightarrow{\mathcal{O}} b = a \overrightarrow{\mathcal{O}} b - (\overrightarrow{\partial} a) \mathcal{O} b$, \mathcal{O} is a spin-isospin operator, and $\mathcal{I} = \text{diag}(1, 1, -2)$ is a diagonal matrix in isospin space. For equivalent Lagrangians in different bases see Refs. [1, 37].

We note as an aside that the relation between these PV dibaryon couplings $g^{(X-Y)}$ and the non-dibaryon couplings $\mathcal{C}^{(X-Y)}$ of Ref. [1] differs from that given in Ref. [2] due to different conventions used in the PC sector. The general expression remains

$$g^{(X-Y)} = \sqrt{8} \frac{\Delta_{s/t}}{y} \mathcal{C}^{(X-Y)}, \quad (\text{IV.2})$$

with Δ_s for $X = {}^1S_0$ and Δ_t for $X = {}^3S_1$, but the values for $\Delta_{s/t}$ and y in the Z-parameterization used here differ from the conventions of Ref. [2].

Higher-order contributions to the Lagrangian of Eq. (IV.1) are suppressed by additional powers of Q . Corrections to S–P wave operators are expected to be suppressed by Q^2 since they contain the same spin-space structure as the terms in Eq. (IV.1), but with two additional derivatives. The effects of different partial waves, such as P–D wave mixing, are suppressed even further.

As in the parity-conserving case, a simplistic application of the power counting suggests that parity-violating 3NIs first start to appear at N²LO. Unlike the PC case, this simplistic

power counting is valid for PV nd scattering; parity-violating corrections to S–P wave transitions from PV 3NIs do not contribute at LO or NLO [38]. The Lagrangian of Eq. (IV.1) is therefore sufficient to determine PV nd scattering up to and including NLO.

V. NEUTRON-PROTON SPIN ROTATION

In the dibaryon formalism, the only diagrams contributing to np spin rotation at LO are the tree-level diagrams shown in Fig. 4. The corresponding non-zero amplitudes are

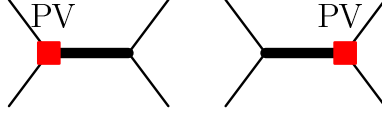


Figure 4: LO PV two-nucleon diagrams. Square: parity-violating two-nucleon vertices.

obtained by using the LO dibaryon propagator of Eq. (III.3):

$$\begin{aligned}
 i\mathcal{M}[n\uparrow p\uparrow \rightarrow n\uparrow p\uparrow] &= i8\sqrt{2}ky \frac{g^{(3S_1-3P_1)}}{\gamma_t + ik}, \\
 i\mathcal{M}[n\downarrow p\downarrow \rightarrow n\downarrow p\downarrow] &= -i8\sqrt{2}ky \frac{g^{(3S_1-3P_1)}}{\gamma_t + ik}, \\
 i\mathcal{M}[n\uparrow p\downarrow \rightarrow n\uparrow p\downarrow] &= i4\sqrt{2}ky \left(\frac{g^{(3S_1-1P_1)}}{\gamma_t + ik} + \frac{g_{(\Delta I=0)}^{(1S_0-3P_0)} - 2g_{(\Delta I=2)}^{(1S_0-3P_0)}}{\gamma_s + ik} \right), \\
 i\mathcal{M}[n\downarrow p\uparrow \rightarrow n\downarrow p\uparrow] &= -i4\sqrt{2}ky \left(\frac{g^{(3S_1-1P_1)}}{\gamma_t + ik} + \frac{g_{(\Delta I=0)}^{(1S_0-3P_0)} - 2g_{(\Delta I=2)}^{(1S_0-3P_0)}}{\gamma_s + ik} \right),
 \end{aligned} \tag{V.1}$$

with k the magnitude of the center-of-mass momentum.

Applying Eq. (II.8) with $\mu = M/2$ for the reduced mass and $k_{\text{lab}} = 2k$, the spin rotation angle for polarized neutrons on a hydrogen target is given by

$$\frac{1}{\rho} \frac{d\phi_{\text{PV}}}{dl} = \frac{M}{4k} \sum_{m_p=\pm\frac{1}{2}} \text{Re}[\mathcal{M}_+(m_p) - \mathcal{M}_-(m_p)], \tag{V.2}$$

where $m_p = \pm\frac{1}{2}$ is the (initial and final) proton polarization. Since the (thermal) external nucleon momentum k appears only in the dibaryon propagators, it is negligible compared to the parameters $\gamma_{s/t}$. With Eq. (V.1), the PV rotation angle for a hydrogen target at LO

is given by

$$\begin{aligned} \frac{1}{\rho} \frac{d\phi_{\text{PV}}^{np}}{dl} \Big|_{\text{LO}} &= 2\sqrt{2\pi M} \left(\frac{2g^{(^3S_1-^3P_1)} + g^{(^3S_1-^1P_1)}}{\gamma_t} + \frac{g_{(\Delta I=0)}^{(^1S_0-^3P_0)} - 2g_{(\Delta I=2)}^{(^1S_0-^3P_0)}}{\gamma_s} \right) \\ &= \left[3.4 \left(2g^{(^3S_1-^3P_1)} + g^{(^3S_1-^1P_1)} \right) - 19.5 \left(g_{(\Delta I=0)}^{(^1S_0-^3P_0)} - 2g_{(\Delta I=2)}^{(^1S_0-^3P_0)} \right) \right] \text{rad MeV}^{-\frac{1}{2}}, \end{aligned} \quad (\text{V.3})$$

where the $g^{(X-Y)}$ carry units of $\text{MeV}^{-3/2}$.

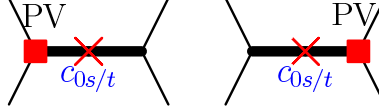


Figure 5: NLO PV two-nucleon diagrams.

Since no new PV operators enter at NLO, as discussed in Sec. IV, the scattering amplitudes at NLO are given by the diagrams in Fig. 5. Using the dibaryon propagator of Eq. (III.5), the LO+NLO result is obtained by multiplying Eq. (V.1) by $\frac{Z_{s/t}+1}{2}$ for each term $\frac{1}{\gamma_{s/t}+ik}$ if the neutron momentum is neglected compared to $\gamma_{s/t}$. This correction is 35% for the $P-^3S_1$ waves and 5% for the $P-^1S_0$ waves, in agreement with the naïve power counting estimate of the EFT($\not{\pi}$) expansion. Our expression up to NLO becomes

$$\begin{aligned} \frac{1}{\rho} \frac{d\phi_{\text{PV}}^{np}}{dl} \Big|_{\text{LO+NLO}} &= \left([4.5 \pm 0.5] \left(2g^{(^3S_1-^3P_1)} + g^{(^3S_1-^1P_1)} \right) \right. \\ &\quad \left. - [18.5 \pm 1.9] \left(g_{(\Delta I=0)}^{(^1S_0-^3P_0)} - 2g_{(\Delta I=2)}^{(^1S_0-^3P_0)} \right) \right) \text{rad MeV}^{-\frac{1}{2}}, \end{aligned} \quad (\text{V.4})$$

where we have conservatively assigned errors of $\mathcal{O}(Q^2) \sim 0.1$.

VI. NEUTRON-DEUTERON SPIN ROTATION

A. nd partial-wave amplitudes at leading order

The parity-violating nd scattering amplitude receives contributions from tree-level (Fig. 6), “one-loop” (Fig. 7), and “two-loop” diagrams (Fig. 8). This nomenclature refers to the number of loops that contain a parity-violating interaction; the strong amplitudes receive contributions from an infinite series of multi-loop diagrams. All graphs use the same interaction kernel, namely the tree-level PV diagrams in the off-shell kinematics specified

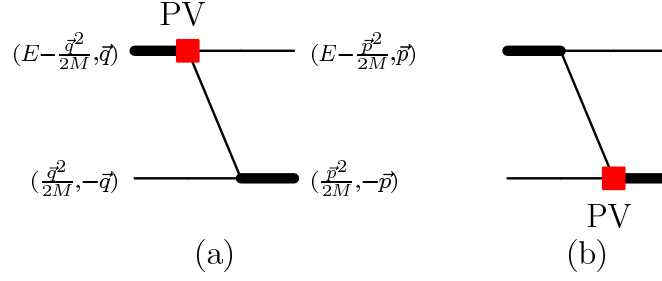


Figure 6: LO tree-level PV diagrams and off-shell kinematics for convolution in Figs. 7 and 8.

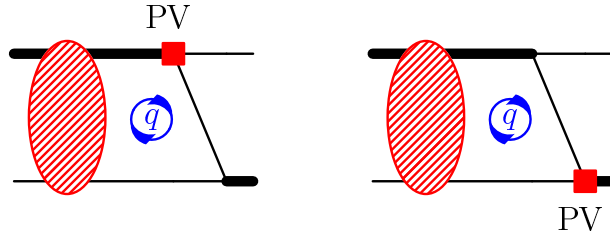


Figure 7: LO “one-loop” PV diagrams. “Time-reversed” contributions (diagrams obtained by reading above ones from right to left) not displayed.

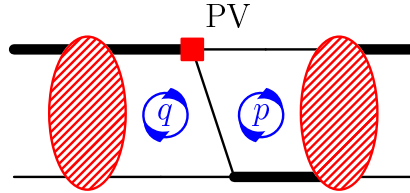


Figure 8: LO “two-loop” PV diagrams. “Time-reversed” (as defined in Fig. 7) contributions not displayed.

in Fig. 6. These are in turn computed using the Lagrangians of Eqs. (III.1) and (IV.1), and with the propagator \mathcal{K} of the exchanged nucleon in Eq. (III.14) as well as the cluster-decomposition version of the dibaryon propagator in Eq. (III.12). Amplitudes between two states with angular momenta L and L' scale as $k^{L+L'}$ for small nucleon momenta, see e.g. [39, p. 381 Eq. (157)]. Since spin-rotation measurements are performed with neutrons with momenta $k \ll 1$ MeV, only transitions between S and P waves contribute at this order, i.e. $L, L' \in \{0; 1\}$. The projectors necessary to filter out specific three-nucleon partial waves are constructed and listed in App. A.

While the PV Lagrangian contains five independent couplings, forward Nd scattering at low energies only depends on three independent (isospin-dependent) linear combinations:

$$\begin{aligned}\mathcal{S}_1 &= 3g^{(3S_1-1P_1)} + 2\tau_3 g^{(3S_1-3P_1)} \quad , \\ \mathcal{S}_2 &= 3g^{(3S_1-1P_1)} - \tau_3 g^{(3S_1-3P_1)} \quad , \\ \mathcal{T} &= 3g_{(\Delta I=0)}^{(1S_0-3P_0)} + 2\tau_3 g_{(\Delta I=1)}^{(1S_0-3P_0)} \quad .\end{aligned}\tag{VI.1}$$

Since the Nd system is an iso-doublet, the PV coupling $g_{(\Delta I=2)}^{(1S_0-3P_0)}$ cannot contribute. Here we are interested in scattering on a neutron, so only the (22) component of the isospin matrix is needed, effectively replacing τ_3 with -1 .

The projected scattering amplitudes of Fig. 6 (a) are:

$$\begin{aligned}
i\mathcal{M}^{(a)} \left[{}^2S_{\frac{1}{2}} \rightarrow {}^2P_{\frac{1}{2}}; q, p \right] &= i \frac{\sqrt{2}yM}{3pq} [2pQ_0(-\mathcal{E}) + qQ_1(-\mathcal{E})] \begin{pmatrix} \mathcal{S}_1 & -\mathcal{T} \\ \mathcal{S}_1 & -\mathcal{T} \end{pmatrix}, \\
i\mathcal{M}^{(a)} \left[{}^2P_{\frac{1}{2}} \rightarrow {}^2S_{\frac{1}{2}}; q, p \right] &= i \frac{\sqrt{2}yM}{3pq} [2pQ_1(-\mathcal{E}) + qQ_0(-\mathcal{E})] \begin{pmatrix} \mathcal{S}_1 & -\mathcal{T} \\ \mathcal{S}_1 & -\mathcal{T} \end{pmatrix}, \\
i\mathcal{M}^{(a)} \left[{}^2S_{\frac{1}{2}} \rightarrow {}^4P_{\frac{1}{2}}; q, p \right] &= i \frac{4yM}{3pq} [2pQ_0(-\mathcal{E}) + qQ_1(-\mathcal{E})] \begin{pmatrix} \frac{\mathcal{S}_1 - \mathcal{S}_2}{3} & \mathcal{T} \\ 0 & 0 \end{pmatrix}, \\
i\mathcal{M}^{(a)} \left[{}^4P_{\frac{1}{2}} \rightarrow {}^2S_{\frac{1}{2}}; q, p \right] &= i \frac{2yM}{3pq} [2pQ_1(-\mathcal{E}) + qQ_0(-\mathcal{E})] \begin{pmatrix} \mathcal{S}_2 & 0 \\ \mathcal{S}_2 & 0 \end{pmatrix}, \\
i\mathcal{M}^{(a)} \left[{}^4S_{\frac{3}{2}} \rightarrow {}^2P_{\frac{3}{2}}; q, p \right] &= i \frac{\sqrt{2}yM}{3pq} [2pQ_0(-\mathcal{E}) + qQ_1(-\mathcal{E})] \begin{pmatrix} \mathcal{S}_2 & 0 \\ \mathcal{S}_2 & 0 \end{pmatrix} Q^r_s, \\
i\mathcal{M}^{(a)} \left[{}^2P_{\frac{3}{2}} \rightarrow {}^4S_{\frac{3}{2}}; q, p \right] &= i \frac{2\sqrt{2}yM}{3pq} [2pQ_1(-\mathcal{E}) + qQ_0(-\mathcal{E})] \begin{pmatrix} \frac{\mathcal{S}_1 - \mathcal{S}_2}{3} & \mathcal{T} \\ 0 & 0 \end{pmatrix} Q^r_s, \\
i\mathcal{M}^{(a)} \left[{}^4S_{\frac{3}{2}} \rightarrow {}^4P_{\frac{3}{2}}; q, p \right] &= -i \frac{2\sqrt{10}yM}{3pq} [2pQ_0(-\mathcal{E}) + qQ_1(-\mathcal{E})] \begin{pmatrix} \frac{\mathcal{S}_1 - \mathcal{S}_2}{3} & 0 \\ 0 & 0 \end{pmatrix} Q^r_s, \\
i\mathcal{M}^{(a)} \left[{}^4P_{\frac{3}{2}} \rightarrow {}^4S_{\frac{3}{2}}; q, p \right] &= -i \frac{2\sqrt{10}yM}{3pq} [2pQ_1(-\mathcal{E}) + qQ_0(-\mathcal{E})] \begin{pmatrix} \frac{\mathcal{S}_1 - \mathcal{S}_2}{3} & 0 \\ 0 & 0 \end{pmatrix} Q^r_s,
\end{aligned} \tag{VI.2}$$

with $E = \frac{3\vec{k}^2}{4M} - \frac{\gamma_t^2}{M} + i\epsilon$ as before and

$$\mathcal{E} = \frac{p^2 + q^2 - ME}{pq}. \tag{VI.3}$$

The structure of these matrices in the cluster space of Eq. (III.11) already appeared in Ref. [38]. The projector $(Q^r_s)^\alpha_\beta = \delta_s^r \delta_\beta^\alpha - \frac{1}{3}(\sigma^r \sigma_s)^\alpha_\beta$ onto the spin quartet is defined in Eq. (A.3). The index α (β) denotes the spin of the outgoing (incoming) nucleon, and r (s) is the spin component of the outgoing (incoming) 3S_1 dibaryon. The diagrams of Fig. 6(b) with the PV interactions on the lower line can be obtained from those of Fig. 6(a) by Hermitian

conjugation in cluster, spin, and isospin space:

$$\mathcal{M}^{(b)}[X \rightarrow Y; q, p]^{r\alpha}_{s\beta} = (\mathcal{M}^{(a)}[Y \rightarrow X; p, q]^{s\beta}_{r\alpha})^\dagger, \quad (\text{VI.4})$$

where X (Y) denotes the partial wave of the incoming (outgoing) state and the spin indices are made explicit. To find the contributions of Fig. 6 to PV scattering, choose the on-shell point $p = q = k$:

$$i\mathcal{M}_{\text{tree}}[X \rightarrow Y; k] = i\mathcal{M}^{(a)}[X \rightarrow Y; k, k] + i\mathcal{M}^{(b)}[X \rightarrow Y; k, k] \quad (\text{VI.5})$$

The “one-loop” and “two-loop” contributions of Figs. 7 and 8 are generated by convoluting the PV tree-level results with the PC amplitudes of Sec. III, following the calculation of higher-order corrections in the PC sector in Ref. [29].

When the PC amplitude is attached to the left of the PV kernel in a “one-loop” diagram, as in Fig. 7, the q_0 integration picks the nucleon pole, $q_0 = -\frac{q^2}{2M} + i\epsilon$, and the angular integration is trivial,

$$i\mathcal{M}_{1\text{-loop, PC left}}^{\text{LO}}[X \rightarrow Y; k] = \sum_{j=a,b} \int_0^\Lambda \frac{dq q^2}{2\pi^2} i\mathcal{M}^{(j)}[X \rightarrow Y; q, k] i\mathcal{D}^{\text{LO}}(E; q) it^{\text{LO}}[X; k, q]. \quad (\text{VI.6})$$

Note that we choose the same UV regulator Λ as in the integral equations for the PC amplitudes, Eqs. (III.13/III.15). When the PC amplitude is attached to the right, the amplitudes are obtained by reading Fig. 7 as if the time direction were reversed:

$$i\mathcal{M}_{1\text{-loop, PC right}}^{\text{LO}}[X \rightarrow Y; k] = \sum_{j=a,b} \int_0^\Lambda \frac{dq q^2}{2\pi^2} it^{\text{LO}}[Y; k, q] i\mathcal{D}^{\text{LO}}(E; q) i\mathcal{M}^{(j)}[X \rightarrow Y; k, q], \quad (\text{VI.7})$$

where we used that the PC amplitudes are time-reversal invariant, i.e. identical when exchanging incoming and outgoing nucleon momenta, $t[X; p, q] = t[X; q, p]$. The “two-loop” convolutions of Fig. 8 are

$$i\mathcal{M}_{2\text{-loop}}^{\text{LO}}[X \rightarrow Y; k] = \sum_{j=a,b} \int_0^\Lambda \frac{dq q^2}{2\pi^2} \int_0^\Lambda \frac{dp p^2}{2\pi^2} it^{\text{LO}}[Y; k, p] i\mathcal{D}^{\text{LO}}(E; p) i\mathcal{M}^{(j)}[X \rightarrow Y; q, p] i\mathcal{D}^{\text{LO}}(E; q) it^{\text{LO}}[X; k, q]. \quad (\text{VI.8})$$

We numerically solve the integral equations for the PC amplitudes t , Eqs. (III.13/III.15), by the Hetherington-Schick method [40] in a Mathematica code, with Λ a hard cutoff corresponding to a step function, as detailed in Ref. [31]. The convolutions for the PV amplitudes

Eqs. (VI.6/VI.7/VI.8) are performed numerically, using again a Mathematica code. The numerical error of $\lesssim 0.1\%$ of these procedures is negligible relative to the systematic uncertainties discussed in Sec. VI E.

Nucleon-deuteron scattering corresponds to the (11) element of the cluster matrix. Multiplication with the LO wave-function normalization factor $\sqrt{\mathcal{Z}_t^{\text{LO}}}$, Eq. (III.7), for each external deuteron leg results in the renormalized, physical scattering amplitude $\mathcal{M}_R^{\text{LO}}$ between partial waves X and Y at nucleon momentum k :

$$\begin{aligned} i\mathcal{M}_R^{\text{LO}}[X \rightarrow Y; k] = & \left(\sqrt{\mathcal{Z}_t^{\text{LO}}}, 0 \right) \left(i\mathcal{M}_{\text{tree}}[X \rightarrow Y; k] + i\mathcal{M}_{1\text{-loop, PC right}}^{\text{LO}}[X \rightarrow Y; k] \right. \\ & \left. + i\mathcal{M}_{1\text{-loop, PC left}}^{\text{LO}}[X \rightarrow Y; k] + i\mathcal{M}_{2\text{-loop}}^{\text{LO}}[X \rightarrow Y; k] \right) \begin{pmatrix} \sqrt{\mathcal{Z}_t^{\text{LO}}} \\ 0 \end{pmatrix} \Big|_{\tau_3 \rightarrow -1}. \end{aligned} \quad (\text{VI.9})$$

B. *nd* partial-wave amplitudes at next-to-leading order

No new PV operators contribute to the NLO amplitudes since higher-order PV interactions are suppressed by at least Q^2 as described in Sec. IV. There are three types of NLO corrections. The first type is given by diagrams with one insertion of an effective-range correction to the dibaryon propagators proportional to c_{0s}/t , see Eq. (III.4). At this order, the momentum-independent PC 3NI parameter $H_0(\Lambda)$ requires an additive adjustment, called $H_0^{\text{NLO}}(\Lambda)$, to recapture the low-energy 3N observable that initially fixed $H_0(\Lambda)$ at leading order. This results in a second type of NLO correction to the *nd* system: diagrams with $H_0^{\text{NLO}}(\Lambda)$ inserted once between LO amplitudes. The third type of corrections comes from the change in the dibaryon wave-function renormalization and is taken into account by replacing $\mathcal{Z}_t^{\text{LO}}$ in the LO PV amplitude of Eq. (VI.9) by $\mathcal{Z}_t^{\text{LO+NLO}}$, see Eq. (III.8).

In a strictly perturbative approach, there are two classes of diagrams at NLO. The class-I diagrams of Fig. 9 are generated when the PC LO amplitudes $t^{\text{LO}}[X; k, q]$ are replaced with the partially-resummed amplitudes $t^{\text{LO+NLO}}[X; k, q]$ in the topologies of the LO PV “one-” and “two-loop” diagrams of Figs. 7 and 8, i.e. $t^{\text{LO}}[X; k, q] \rightarrow t^{\text{LO+NLO}}[X; k, q]$ at each occurrence in Eqs. (VI.6/VI.7/VI.8), see Fig. 10. In addition to the NLO class-I diagrams, the amplitudes obtained from Fig. 10 also contain all LO contributions as well as a partial resummation of higher-order effects. In analogy to the notation at LO, the resulting contributions are called $\mathcal{M}_{1\text{-loop, PC left}}^{\text{LO+NLO, class-I}}[X \rightarrow Y; k]$, $\mathcal{M}_{1\text{-loop, PC right}}^{\text{LO+NLO, class-I}}[X \rightarrow Y; k]$,

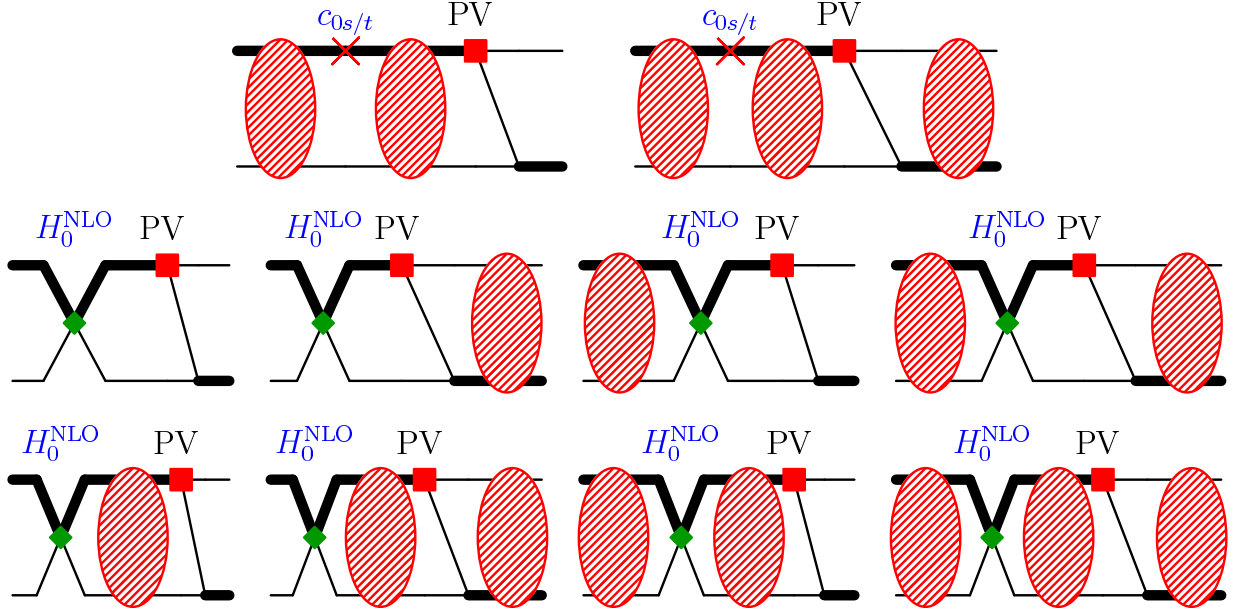


Figure 9: Class-I diagrams. Diagrams with the PV vertex on the lower line as well as “time-reversed” contributions not displayed.

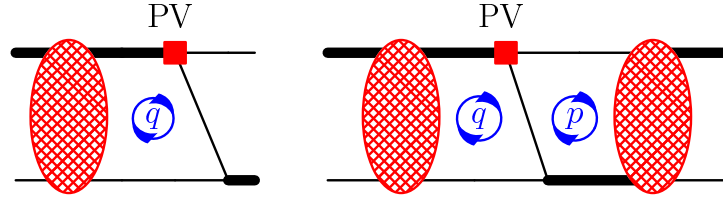


Figure 10: Reformulation of the class-I diagrams of Fig. 9 using the amplitudes $t^{\text{LO+NLO}}$ of Fig. 2. This also replaces the LO PV contributions of Figs. 7 and 8. Diagrams with the PV vertex on the lower line as well as “time-reversed” contributions not displayed.

and $\mathcal{M}_{2\text{-loop}}^{\text{LO+NLO, class-I}}[X \rightarrow Y; k]$. This approach has computational advantages since it avoids diagrams with up to four numerical integrations and convolutions with parity-conserving LO full-off-shell amplitudes $t^{\text{LO}}[{}^{2S+1}L_J; p, q]$, $p, q \neq k$. In addition, the diagrams in class I contain divergences, studied by Refs. [38, 41, 42], that in a strictly perturbative calculation are cancelled by corresponding contributions in class-II diagrams, to be discussed shortly. These divergences are challenging to treat numerically, but are avoided in the approach used here. The amplitudes corresponding to the diagrams of Fig. 10 are individually renormalized; each diagram approaches a unique and finite limit as the cutoff is removed, $\Lambda \rightarrow \infty$.

Diagrams that are not generated by the replacement $t^{\text{LO}}[X; k, q] \rightarrow t^{\text{LO+NLO}}[X; k, q]$ in Figs. 7 and 8 are referred to as “class-II” diagrams and are shown in Fig. 11. The

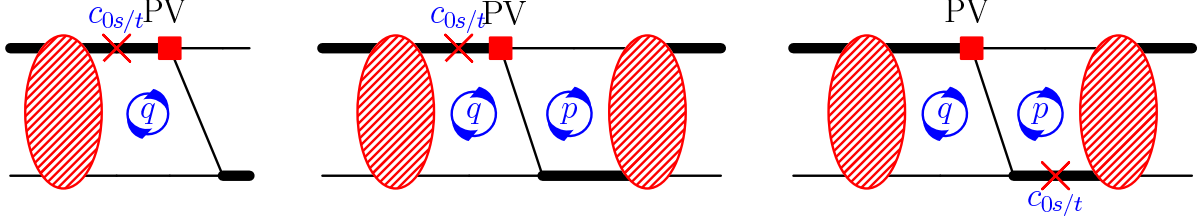


Figure 11: Class-II diagrams. As discussed in the text, the PC amplitudes are taken as $t^{\text{LO+NLO}}$ for ${}^2\text{S}_{\frac{1}{2}}$ and ${}^4\text{S}_{\frac{3}{2}}$, and as t^{LO} for ${}^2\text{P}_J$ and ${}^4\text{P}_J$. Diagrams with the PV vertex on the lower line as well as “time-reversed” contributions not displayed.

corresponding amplitudes are given by

$$\text{i}\mathcal{M}_{1\text{-loop, PC left}}^{\text{NLO, class-II}}[X \rightarrow Y; k] = \sum_{j=a,b} \int_0^\Lambda \frac{dq q^2}{2\pi^2} \text{i}\mathcal{M}^{(j)}[X \rightarrow Y; q, k] \text{i}\mathcal{D}^{\text{NLO}}(E; q) \text{it}[X; k, q] , \quad (\text{VI.10})$$

$$\text{i}\mathcal{M}_{1\text{-loop, PC right}}^{\text{NLO, class-II}}[X \rightarrow Y; k] = \sum_{j=a,b} \int_0^\Lambda \frac{dq q^2}{2\pi^2} \text{it}[Y; k, q] \text{i}\mathcal{D}^{\text{NLO}}(E; q) \text{i}\mathcal{M}^{(j)}[X \rightarrow Y; k, q] , \quad (\text{VI.11})$$

$$\begin{aligned} \text{i}\mathcal{M}_{2\text{-loop}}^{\text{NLO, class-II}}[X \rightarrow Y; k] = & \quad (\text{VI.12}) \\ & \sum_{j=a,b} \int_0^\Lambda \frac{dq q^2}{2\pi^2} \int_0^\Lambda \frac{dp p^2}{2\pi^2} \text{it}[Y; k, p] \left[\text{i}\mathcal{D}^{\text{LO}}(E; p) \text{i}\mathcal{M}^{(j)}[X \rightarrow Y; q, p] \text{i}\mathcal{D}^{\text{NLO}}(E; q) \right. \\ & \quad \left. + \text{i}\mathcal{D}^{\text{NLO}}(E; p) \text{i}\mathcal{M}^{(j)}[X \rightarrow Y; q, p] \text{i}\mathcal{D}^{\text{LO}}(E; q) \right] \text{it}[X; k, q] . \end{aligned}$$

Since the kernel of these convolutions is now already NLO, it appears that the LO PC amplitudes $t^{\text{LO}}[X; k, q]$ can be used directly. This is the strategy implemented for the PC P-wave amplitudes.

For a convolution of the class-II diagrams involving the LO PC ${}^2\text{S}_{\frac{1}{2}}$ -wave amplitude the situation is more complicated. It was demonstrated on general grounds in Ref. [38], and confirmed numerically here that when using t^{LO} the “one-loop” amplitudes diverge logarithmically, and the “two-loop” amplitudes diverge as $q^{0.23\dots}$; see App. B. These are

not divergences that are removed by additional parity-violating 3NIs at NLO [38]. In a strictly perturbative calculation in the PC sector, the 3NI H_0^{NLO} absorbs a linear divergence generated by insertions of the effective-range term [41, 42]. It is this linear divergence in H_0^{NLO} which, when inserted next to a PV interaction (see class-I diagrams in Fig. 9), would renormalize the divergence in the class-II contributions. However, in the partially-resummed formalism used here for the class-I diagrams $H_0^{\text{LO+NLO}}$ does not diverge linearly as $\Lambda \rightarrow \infty$, see Fig. 3, since the high-off-shell momentum part of the scattering equation, and hence of the amplitude, becomes softer. Therefore, the treatment of class-I diagrams using the partial resummation technique, see Fig. 10, removes those divergences from the class-I diagrams. This in turn means that the class-I diagrams do not renormalize the divergent class-II contributions, so that the divergences in the class-II diagrams require separate renormalization. By using the renormalized (partially-resummed) PC amplitude $t^{\text{LO+NLO}}[{}^2\text{S}_{\frac{1}{2}}; k, q]$ for the ${}^2\text{S}_{\frac{1}{2}}$ channel the UV behavior of the class-II diagrams is changed and no divergences appear. As demonstrated below in Fig. 12, this leads to renormalized, cutoff-independent PV amplitudes. We therefore choose the renormalized PC amplitude $t^{\text{LO+NLO}}[{}^2\text{S}_{\frac{1}{2}}; k, q]$ for this channel.

We also choose the LO+NLO version for the PC ${}^4\text{S}_{\frac{3}{2}}$ -wave amplitude in the class-II diagrams. This is not required by renormalization, as the loop-integrations in Eqs. (VI.10/VI.11/VI.12) converge well in this channel, see again Ref. [38]. However, neutron spin-rotation in deuterium is particularly sensitive to the scattering lengths of the nd system since it is a process essentially at zero kinetic energy. It is therefore important to reproduce the experimental values of the scattering lengths. In particular, the ${}^4\text{S}_{\frac{3}{2}}$ scattering length is a factor of 10 larger than the ${}^2\text{S}_{\frac{1}{2}}$ one, so it will most likely dominate spin-rotation observables. At LO in the Z-parameterization used here, the ${}^4\text{S}_{\frac{3}{2}}$ scattering length of 5.1 fm would require a 25 percent correction to achieve the experimental value of $[6.35 \pm 0.02]$ fm [36], while the NLO amplitude leads to 6.4 fm, in close agreement with the experimental value, see Ref. [31]. We therefore use the NLO PC amplitude $t^{\text{LO+NLO}}[{}^4\text{S}_{\frac{3}{2}}; k, q]$ for this channel. This choice does not violate the power counting of the theory and yet improves the utility of our result.

To summarize, the PC amplitudes used in Eqs. (VI.10/VI.11/VI.12) are:

$$t[X; k, q] = \begin{cases} t^{\text{LO+NLO}}[X; k, q] & \text{for } X \in \{^2\text{S}_{\frac{1}{2}}, ^4\text{S}_{\frac{3}{2}}\}, \\ t^{\text{LO}}[X; k, q] & \text{for } X \in \{^2\text{P}, ^4\text{P}\}. \end{cases} \quad (\text{VI.13})$$

Further details and comparisons to other choices are discussed in App. B.

The renormalized LO+NLO PV amplitudes are obtained by summing and multiplying with the LO+NLO wave-function renormalization:

$$\begin{aligned} i\mathcal{M}_{\text{R}}^{\text{LO+NLO}}[X \rightarrow Y; k] = & \left(\sqrt{\mathcal{Z}_t^{\text{LO+NLO}}}, 0 \right) \left(i\mathcal{M}_{\text{tree}}[X \rightarrow Y; k] \right. \\ & + i\mathcal{M}_{1\text{-loop, PC left}}^{\text{LO+NLO, class-I}}[X \rightarrow Y; k] + i\mathcal{M}_{1\text{-loop, PC left}}^{\text{NLO, class-II}}[X \rightarrow Y; k] \\ & + i\mathcal{M}_{1\text{-loop, PC right}}^{\text{LO+NLO, class-I}}[X \rightarrow Y; k] + i\mathcal{M}_{1\text{-loop, PC right}}^{\text{NLO, class-II}}[X \rightarrow Y; k] \\ & \left. + i\mathcal{M}_{2\text{-loop}}^{\text{LO+NLO, class-I}}[X \rightarrow Y; k] + i\mathcal{M}_{2\text{-loop}}^{\text{NLO, class-II}}[X \rightarrow Y; k] \right) \begin{pmatrix} \sqrt{\mathcal{Z}_t^{\text{LO+NLO}}} \\ 0 \end{pmatrix} \end{aligned} \quad (\text{VI.14})$$

Finally, we reiterate that these amplitudes are complete up to NLO, but also contain some higher-order contributions. The PC amplitudes $t^{\text{LO+NLO}}$ used are partially resummed. In addition, we choose to multiply the entire LO+NLO amplitude by the LO+NLO wave-function renormalization, rather than the LO PV amplitude $\mathcal{M}_{\text{R}}^{\text{LO}}$ by $\mathcal{Z}^{\text{LO+NLO}}$ and the NLO correction $(\mathcal{M}_{\text{R}}^{\text{LO+NLO}} - \mathcal{M}_{\text{R}}^{\text{LO}})$ only by \mathcal{Z}^{LO} . It has been demonstrated repeatedly that this speeds up convergence since the larger-than-usual wave-function renormalization correction at NLO is expected to be the dominant correction to insertions of higher-dimension operators; see e.g. Refs. [18, 31, 33].

The computational effort can be halved by taking advantage of the fact that the individual tree-level amplitudes $\mathcal{M}^{(a)}$ and $\mathcal{M}^{(b)}$ are Hermitian conjugates, Eq. (VI.4), and that the PC amplitudes are time-reversal invariant, $t[X; p, q] = t[X; q, p]$. The amplitudes of partial waves $X \rightarrow Y$ and $Y \rightarrow X$ are therefore related:

$$\mathcal{M}_{1\text{-loop, PC right}}[X \rightarrow Y; k] = (\mathcal{M}_{1\text{-loop, PC left}}[Y \rightarrow X; k])^\dagger, \quad (\text{VI.15})$$

$$\mathcal{M}_{1\text{-loop}}[X \rightarrow Y; k] = (\mathcal{M}_{1\text{-loop}}[Y \rightarrow X; k])^\dagger, \quad (\text{VI.16})$$

$$\mathcal{M}_{2\text{-loop}}[X \rightarrow Y; k] = (\mathcal{M}_{2\text{-loop}}[Y \rightarrow X; k])^\dagger, \quad (\text{VI.17})$$

$$\mathcal{M}_{\text{R}}[X \rightarrow Y; k] = \mathcal{M}_{\text{R}}[Y \rightarrow X; k]. \quad (\text{VI.18})$$

C. Cutoff independence of partial-wave amplitudes

Numerically, it is difficult to perform some of the integrations at very low energies. However, between $k = 0.01$ MeV and 10 MeV the amplitudes of the nd system deviate from the linear relation only at the percent-level. For the spin rotation angle, the relevant quantity is \mathcal{M}_R/k , see Eq. (II.8). The difference in \mathcal{M}_R/k at $k = 1$ MeV and 0.01 MeV is less than 0.3%. All results quoted are for $k = 1$ MeV.

For the analysis of the cutoff dependence of the partial-wave amplitudes, we decompose them in terms of the PV interactions \mathcal{S}_1 , \mathcal{S}_2 , and \mathcal{T} of Eq. VI.1:

$$\begin{aligned} \frac{\text{Re}[\mathcal{M}_R[X \rightarrow Y; k]]}{k} = & d[X \rightarrow Y; \mathcal{S}_1](\Lambda) \mathcal{S}_1 \\ & + d[X \rightarrow Y; \mathcal{S}_2](\Lambda) \mathcal{S}_2 + d[X \rightarrow Y; \mathcal{T}](\Lambda) \mathcal{T} . \end{aligned} \quad (\text{VI.19})$$

In Figs. 12 and 13, the dependence of the functions d on the cutoff Λ used in the PC 3N integral equations Eqs. (III.13/III.15) and in the convolutions of Secs. VIA and VIB is shown for each partial-wave and order. Since a unique, finite limit exists as $\Lambda \rightarrow \infty$, the result is properly renormalized in each partial wave. These results confirm the theoretical findings of Ref. [38] that no PV 3NI is required at LO and NLO. Comparison with Fig. 3 also shows that at both LO and NLO the physical amplitudes are smooth even where the 3NI H_0 diverges.

A small kink in the cutoff dependence of the partial wave amplitudes is seen at NLO for $\Lambda \approx 3000$ MeV. It is evident in all partial waves, and so is not related to the renormalization of the 3NI H_0 of the $^2\text{S}_{1/2}$ -wave. The phenomenon appears only at cutoffs well beyond the breakdown scale of 200 MeV and hence does not have any impact on our final result.

D. Translating partial-wave amplitudes into neutron-spin rotation predictions

For computational convenience, the calculations so far have been performed in a partial-wave basis. However, in order to obtain the spin rotation angle, we need to determine the forward scattering amplitude for specific neutron helicity states. Recall that in the kinematics of Sec. III, the incident and outgoing nucleons have momentum $-\vec{k} = -k\vec{e}_z$, so that an incoming neutron $N^{a\alpha}(-\vec{k})$ with positive helicity corresponds to choosing the spin and isospin components $\alpha = 2$, $a = 2$. The relation to the results in the partial-wave basis

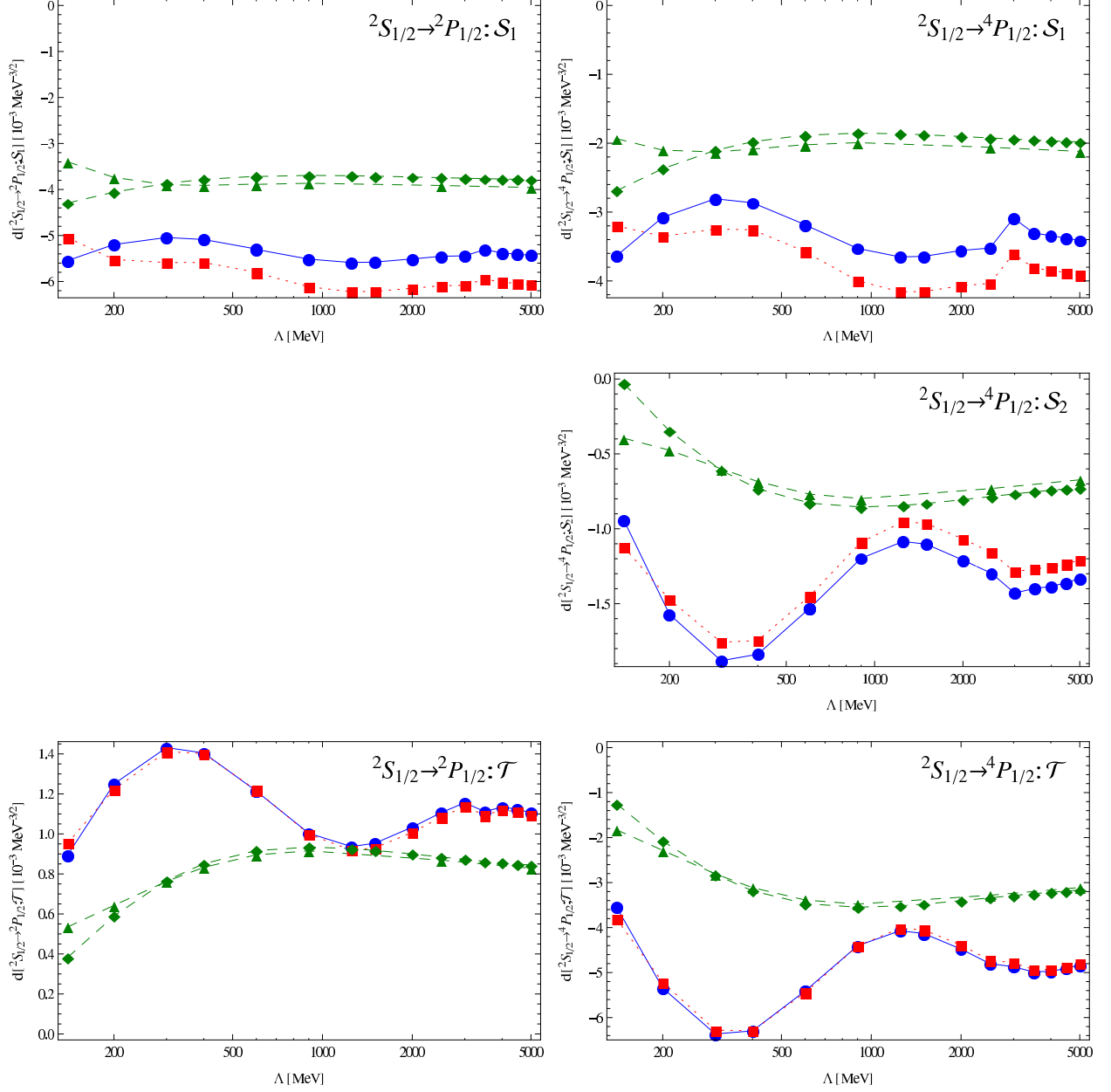


Figure 12: Cutoff dependence of the functions $d[{}^2S_{1/2} \rightarrow Y; \text{coupling}](\Lambda)$, Eq. (VI.19). Columns (left to right): partial waves ${}^2S_{1/2} \rightarrow {}^2P_{1/2}$, ${}^2S_{1/2} \rightarrow {}^4P_{1/2}$; rows (top to bottom): coefficients of \mathcal{S}_1 , \mathcal{S}_2 , \mathcal{T} . \blacklozenge (dashed lines): LO, 3NI H_0 determined from nd ${}^2S_{1/2}$ -scatt. length; \blacktriangle (dashed lines): LO, 3NI from triton binding energy; \bullet (solid lines): NLO, 3NI from ${}^2S_{1/2}$ -scatt. length; \blacksquare (dotted lines): NLO, 3NI from triton binding energy. The linear extrapolations are only meant to guide the eye. Notice the different scales on the vertical axes. Amplitudes which are identically zero are not displayed.

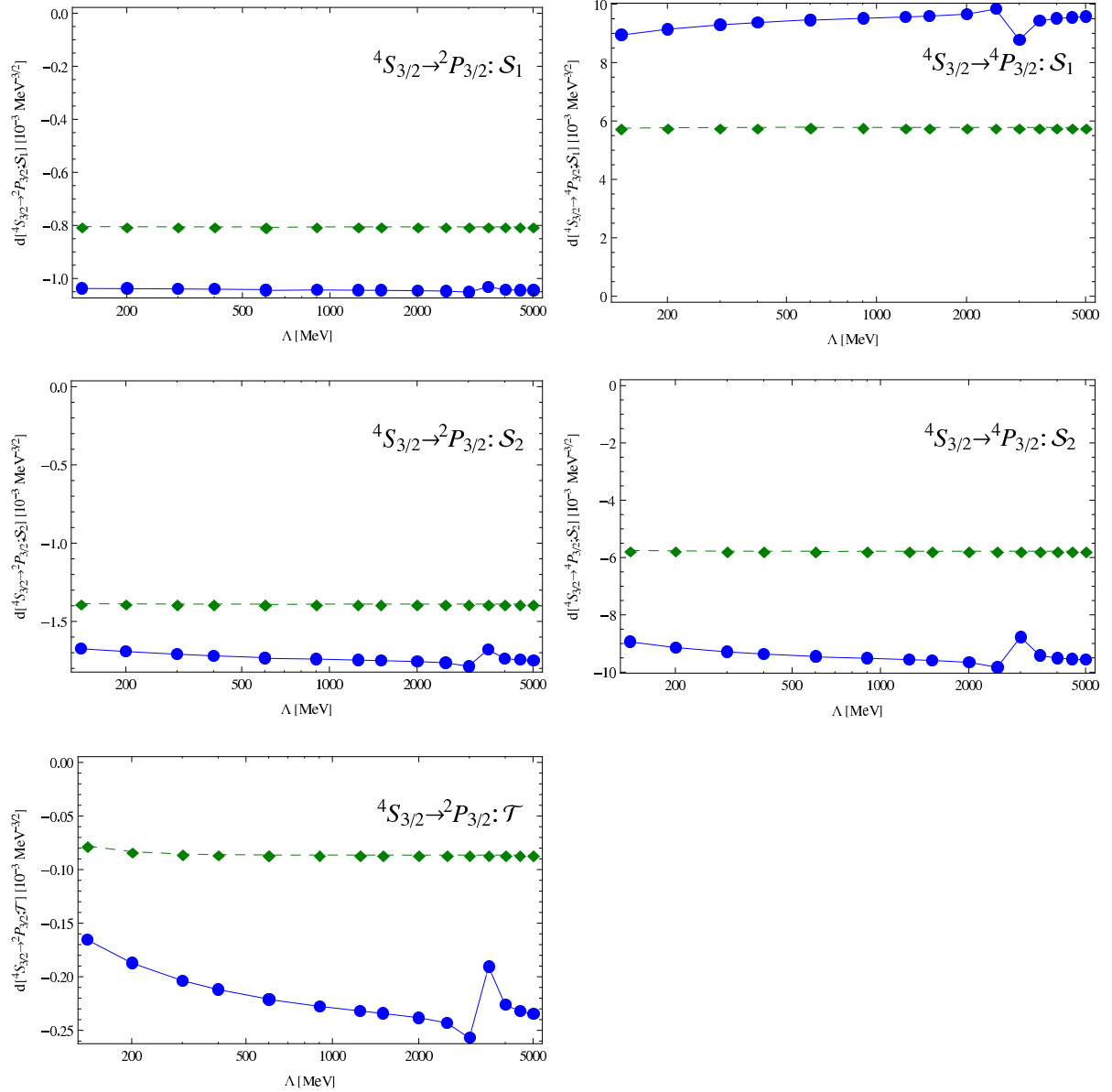


Figure 13: Cutoff dependence of the functions $d[{}^4S_{\frac{3}{2}} \rightarrow Y; \text{coupling}](\Lambda)$, Eq. (VI.19). Columns (left to right): partial waves ${}^4S_{\frac{3}{2}} \rightarrow {}^2P_{\frac{3}{2}}$, ${}^4S_{\frac{3}{2}} \rightarrow {}^4P_{\frac{3}{2}}$; rows (top to bottom): coefficients of \mathcal{S}_1 , \mathcal{S}_2 , \mathcal{T} . \blacklozenge (dashed lines): LO; \bullet (solid lines): NLO. Comments as in Fig. 12.

is obtained by inserting a complete set of projection operators:

$$\langle d_j N_{b\beta}(-\vec{k}) | \mathcal{M} | d^i N^{a\alpha}(-\vec{k}) \rangle = \sum_{XY} \langle d_j N_{b\beta}(-\vec{k}) | Y \rangle \langle Y | \mathcal{M} | X \rangle \langle X | d^i N^{a\alpha}(-\vec{k}) \rangle, \quad (\text{VI.20})$$

where $\langle Y | \mathcal{M} | X \rangle = \mathcal{M}_R[X \rightarrow Y]$ are the partial-wave amplitudes calculated above. The sum over X, Y stands for all partial waves including spin and isospin polarizations.

Using the three-body projectors $\mathcal{P}[X]$ constructed in App. A from Eq. (A.14), the partial-wave projected matrix elements of the neutron-deuteron state are

$$\langle X = ({}^{2S+1}L_J; b\beta\{M\}) | d^i N^{a\alpha}(-\vec{k}) \rangle = \left[(\mathcal{P}^{\{M\}}_i [{}^{2S+1}L_J])^{b\beta}_{a\alpha} \right]_{11}, \quad (\text{VI.21})$$

with appropriate vector and spinor indices $\{M\}$. The outer bracket $[\cdot]_{11}$ indicates that only the (11)-entry of the cluster-decomposition matrix is physically allowed. As an example, the projection onto the ${}^4\text{P}_{\frac{1}{2}}$ -wave is

$$\langle {}^4\text{P}_{\frac{1}{2}} | d_i N^{a\alpha}(-k\vec{e}_k) \rangle = \sqrt{\frac{3}{2}} (Q^3_i)^\beta{}_\alpha \delta_a^b, \quad (\text{VI.22})$$

where the indices β, b are needed to specify the spinor and isospinor magnetic quantum numbers of the ${}^4\text{P}_{\frac{1}{2}}$ state, and $\vec{e}_k = (0, 0, 1)$ for forward-scattering. The positive-helicity neutron-deuteron amplitude is then:

$$\mathcal{M}_+ = \sum_{XY} \mathcal{M}_R[X \rightarrow Y] \frac{1}{3} \sum_{i \in \{0; \pm 1\}} \left[\left((\mathcal{P}^{\{M\}}_i)^{iA}[Y] \right)^\dagger \mathcal{P}^{\{M\}}_{iA}[X] \right]_{\beta=2, \alpha=2; a=2, b=2} \Big|_{11}. \quad (\text{VI.23})$$

Note that the iso-vector index A is irrelevant for the final (11)-component of the cluster-decomposition matrix. This formula can also be understood as a decomposition into the reduced matrix elements, represented by the amplitudes $\mathcal{M}_R[X \rightarrow Y]$ calculated above, and the equivalent of Clebsch-Gordan coefficients weighting the various partial waves. The negative-helicity amplitude is $\mathcal{M}_- = -\mathcal{M}_+$. Using the partial-wave projectors of App. A leads to our final result for the neutron spin-rotation in deuterium from Eq. (II.8) with $\mu = 2M/3$ for the reduced mass:

$$\begin{aligned} \frac{1}{\rho} \frac{d\phi_{\text{PV}}^{nd}}{dl} = & \frac{2M}{6k} \frac{4}{9} \text{Re} \left[\mathcal{M}_R[{}^2\text{S}_{\frac{1}{2}} \rightarrow {}^2\text{P}_{\frac{1}{2}}; k] - 2\sqrt{2} \mathcal{M}_R[{}^2\text{S}_{\frac{1}{2}} \rightarrow {}^4\text{P}_{\frac{1}{2}}; k] \right. \\ & \left. - 4\mathcal{M}_R[{}^4\text{S}_{\frac{3}{2}} \rightarrow {}^2\text{P}_{\frac{3}{2}}; k] - 2\sqrt{5} \mathcal{M}_R[{}^4\text{S}_{\frac{3}{2}} \rightarrow {}^4\text{P}_{\frac{3}{2}}; k] \right], \end{aligned} \quad (\text{VI.24})$$

where the amplitudes for P to S wave transitions are taken into account by using the relations of Eq. (VI.18).

E. Numerical nd spin rotation result and error estimates

For the detailed discussion of theoretical errors below, we decompose the spin-rotation result of Eq. (VI.24) in terms of functions $c[(X-Y)](\Lambda)$ which multiply the PV interactions:

$$\frac{1}{\rho} \frac{d\phi_{\text{PV}}^{nd}}{dl} = c[({}^3\text{S}_1 - {}^1\text{P}_1)](\Lambda) g^{({}^3\text{S}_1 - {}^1\text{P}_1)} + \tau_3 c[({}^3\text{S}_1 - {}^3\text{P}_1)](\Lambda) g^{({}^3\text{S}_1 - {}^3\text{P}_1)} + c[\mathcal{T}](\Lambda) \mathcal{T} \quad (\text{VI.25})$$

The isospin matrix τ_3 is replaced by -1 for neutron spin-rotation, and $\mathcal{T} = 3g_{(\Delta I=0)}^{(^1S_0-^3P_0)} + 2\tau_3 g_{(\Delta I=1)}^{(^1S_0-^3P_0)}$, see Eq. (VI.1). Figure 14 shows the cutoff dependence of the functions $c[(X - Y)](\Lambda)$. As expected from the discussion of the cutoff dependence of the partial-wave amplitudes, the result for the spin-rotation angle is also properly renormalized.

The final result for neutron spin-rotation in deuterium is:

$$\begin{aligned} \frac{1}{\rho} \frac{d\phi_{\text{PV}}^{nd}}{dl} = & \left([8.0 \pm 0.8] g^{(^3S_1-^1P_1)} + [17.0 \pm 1.7] g^{(^3S_1-^3P_1)} \right. \\ & \left. + [2.3 \pm 0.5] \left(3g_{(\Delta I=0)}^{(^1S_0-^3P_0)} - 2g_{(\Delta I=1)}^{(^1S_0-^3P_0)} \right) \right) \text{rad MeV}^{-\frac{1}{2}}, \end{aligned} \quad (\text{VI.26})$$

where the estimate of the residual theoretical uncertainties is justified below. It will turn out that this estimate is rather conservative; drawing from the experience in calculations of PC 3N observables using the Z -parameterization, theoretical systematic errors might be estimated to be on the order of 3%, see e.g. [31, 43]. For now, we note that the theoretical errors of 10% to 20% are comparable to the statistical and systematic errors expected of the most ambitious planned experiments.

We use three methods to estimate theoretical uncertainties, with the EFT($\not\Lambda$) parameter $Q \approx \frac{1}{3}$ as a conservative value for typical momenta in the Nd system on the order of γ_t (see Ref. [31]).

- (i) At NLO, higher orders should contribute corrections of order $Q^2 \approx 0.1$ to the total result.
- (ii) Since EFT($\not\Lambda$) is not valid at high momentum, a residual dependence of observables on momentum modes above the breakdown scale $\bar{\Lambda} \sim 200$ MeV is an indicator of the size of higher-order corrections. Varying the momentum cutoff Λ in the Faddeev equations and convolutions of the 3N system from the breakdown scale to higher values provides an estimate of N²LO effects. The parameters $g^{(X-Y)}$ of the PV Lagrangian Eq. (IV.1) are independent of the regularization scale Λ . Therefore, the $c[(X - Y)](\Lambda)$ of the spin-rotation results of Eq. (VI.25) must also be cutoff-independent up to higher-order effects. In particular, this implies that these coefficients should approach a unique, finite limit as the cutoff is removed. As in a variety of previous calculations in the 3N system, we consider cutoff-variations from $\Lambda = 200$ MeV to 5000 MeV, see e.g. Refs. [31, 35].

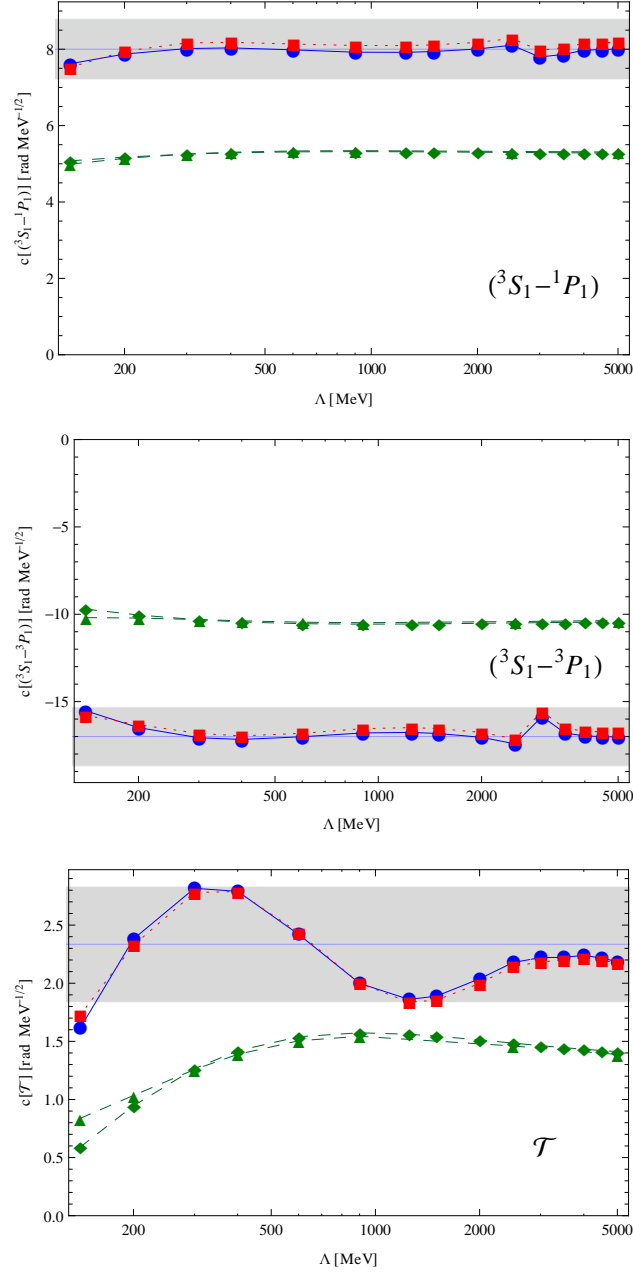


Figure 14: Cutoff dependence of the functions $c[(X - Y)](\Lambda)$ for the neutron spin-rotation angle in deuterium, (VI.25). Notation as in Fig. 12. Grey band: estimated theoretical uncertainties as described in Eq. (VI.26). The linear extrapolations are only meant to guide the eye. Notice the different scales on the vertical axes.

- (iii) Finally, the size of higher-order effects can be assessed by using different low-energy data to determine the PC parameters of EFT(\not{n}). Since we chose Z-parameterization

precisely because of its well-established improved convergence, we do not vary parameters of the NN system, e.g. by replacing $(Z_{s/t} - 1)$ at NLO by the effective ranges. On the other hand, the strength of the PC 3NI H_0 can for example be determined from the nd scattering length of the $^2S_{\frac{1}{2}}$ -wave, or from the triton binding energy. The difference between both approaches is again a measure of N²LO effects, i.e. expected to be on the order of $Q^2 \approx 0.1$.

Note that methods (ii) and (iii) do not apply to the 2N system. We will base our error-estimate for the nd spin-rotation coefficients on the most conservative of the above methods.

The NLO corrections are as large as 70% relative to the LO result. The size of this correction stems from the unnaturally large residue of the deuteron pole, $Z_t - 1 \approx 0.7$, in Z-parameterization. However, once this effect is taken into account, convergence at N²LO and higher is actually improved [18, 31, 33]. Different inputs to determine the PC 3NI affect only the $^2S_{\frac{1}{2}} \rightarrow X$ partial-wave amplitudes. At NLO, this can lead to a change of up to 15% in the amplitudes $\mathcal{M}_R[^2S_{\frac{1}{2}} \rightarrow Y; k]$, in line with the error-estimate criterion (iii).

In the functions $c[(X - Y)](\Lambda)$ multiplying the PV couplings $g^{(^3S_1 - ^1P_1)}$ and $g^{(^3S_1 - ^3P_1)}$, Fig. 14, contributions involving the $^2S_{\frac{1}{2}}$ -wave are doubly suppressed relative to those which contain the $^4S_{\frac{3}{2}}$ -wave. Not only are their relative weights in Eq. (VI.24) small, they are also small in absolute size, as seen from the fact that the $^2S_{\frac{1}{2}}$ -wave scattering length itself is a factor of ≈ 10 smaller than the $^4S_{\frac{3}{2}}$ one. Therefore, applying criterion (iii) leads to very small variations. Varying the cutoff $\Lambda \in [200; 5000]$ MeV, criterion (ii), produces a range at NLO of $c[(^3S_1 - ^1P_1)](\Lambda) = [7.8 \dots 8.1]$ rad MeV $^{-\frac{1}{2}}$ and $c[(^3S_1 - ^3P_1)](\Lambda) = -[16.5 \dots 17.4]$ rad MeV $^{-\frac{1}{2}}$. For error-estimate criterion (i), i.e. $Q^2 \approx 0.1$ of the total result, corrections are ± 0.8 rad MeV $^{-\frac{1}{2}}$ and ± 1.7 rad MeV $^{-\frac{1}{2}}$, significantly larger than the estimate from varying Λ . We therefore adopt the range from criterion (i) as a conservative estimate of the theoretical uncertainties in these coefficients. Overall, the amplitude $\mathcal{M}_R[^4S_{\frac{3}{2}} \rightarrow ^4P_{\frac{3}{2}}]$ dominates $c[(^3S_1 - ^3P_1)](\Lambda)$, providing more than 80% of its total value.

Due to symmetries, the function $c[\mathcal{T}](\Lambda)$ does not receive any contributions from the $^4S_{\frac{3}{2}} \rightarrow ^4P_{\frac{3}{2}}$ channel, and the amplitude $\mathcal{M}_R[^4S_{\frac{3}{2}} \rightarrow ^2P_{\frac{3}{2}}]$ is very small. The $^2S_{\frac{1}{2}} \rightarrow ^4P_{\frac{1}{2}}$ amplitude thus dominates $c[\mathcal{T}](\Lambda)$. Since this amplitude does not depend significantly on the input used to determine the PC 3NI, criterion (iii) significantly underestimates the theoretical uncertainty of the NLO calculation. Cutoff-variation, criterion (ii), is significant in this channel, mapping out the range $c[\mathcal{T}](\Lambda) = [1.8 \dots 2.8]$ rad MeV $^{-\frac{1}{2}}$, while criterion (i)

provides an error-estimate of only $\pm 0.3 \text{ rad MeV}^{-\frac{1}{2}}$. We therefore adopt the variation from the cutoff changes as a conservative estimate of the theoretical uncertainties. While this error is $\approx 20\%$, the magnitude of $c[\mathcal{T}](\Lambda)$ is at most a third of the other two $c[(X - Y)](\Lambda)$. If there are no accidental cancellations or significant differences in the magnitudes of the PV couplings themselves, the overall contribution of $c[\mathcal{T}](\Lambda)$ to the spin rotation angle is expected to be small.

VII. ROTATION ANGLE ESTIMATES AND COMPARISONS

Our results for np and nd spin rotation are given in terms of the LECs $g^{(X-Y)}$ of the Lagrangian (IV.1). As discussed in the Introduction, these couplings are not predicted by the EFT, but can be estimated on dimensional grounds. Since on the microscopic level the dominant PV process stems from a single weak gauge boson exchange, the PV NN interactions are suppressed relative to the PC ones by a factor $\sim \frac{\gamma_t^2}{M_W^2}$, where γ_t is taken as a typical low-momentum scale. As in the PC interactions between two nucleons and the auxiliary dibaryon field in Eq. (III.2), an overall factor of $\sqrt{\frac{4\pi}{M}}$ should be included. In order to match the dimensionality $[\text{MeV}^{-\frac{3}{2}}]$ of the couplings $g^{(X-Y)}$, an additional inverse mass dimension enters. Since the PV couplings used here are renormalization-group invariant and encode short-distance physics, the mass scale can only be set by the breakdown scale $\bar{\Lambda} \approx m_\pi \approx 140 \text{ MeV}$ of EFT($\not{\pi}$). Overall, therefore, we expect the magnitude of the PV couplings to be of order

$$|g^{(X-Y)}| \sim \sqrt{\frac{4\pi}{M}} \frac{1}{\bar{\Lambda}} \left(\frac{\gamma_t}{M_W} \right)^2 \approx 10^{-10} \text{ MeV}^{-\frac{3}{2}}. \quad (\text{VII.1})$$

An estimate which is compatible with this number may be obtained by appealing to Ref. [1], where a value for the combination of couplings involved in PV $\vec{p}p$ scattering at 13.6 MeV [44] was extracted. (Asymmetries measured at higher energies are not within the realm of validity of EFT($\not{\pi}$).) Using this value as an estimate of all LECs,

$$|g^{(X-Y)}| \approx 2 \times 10^{-11} \text{ MeV}^{-\frac{3}{2}} \quad (\text{VII.2})$$

in our conventions. Note that these are only rough estimates.

With these values for the magnitude of the PV couplings and a target density of $\rho \approx$

10^{23} cm^{-3} , the magnitude of the spin-rotation signal in hydrogen of Eq. (V.4) is

$$\left| \frac{d\phi_{\text{PV}}^{np}}{dl} \right| \approx [10^{-7} \dots 10^{-6}] \frac{\text{rad}}{\text{m}} . \quad (\text{VII.3})$$

Analogously, the magnitude of the spin-rotation signal in deuterium of Eq. (VI.26) is roughly

$$\left| \frac{d\phi_{\text{PV}}^{nd}}{dl} \right| \approx [10^{-7} \dots 10^{-6}] \frac{\text{rad}}{\text{m}} . \quad (\text{VII.4})$$

We stress again that – without reliable values of the PV parameters – these results are dimensional, order-of-magnitude estimates and may well be off by factors of 10 or more.

Another order-of-magnitude estimate can be obtained by using the parameter set of Ref. [26] extracted from the DDH “best estimates”; using these values (Eq. (31) of Ref. [26]) and adjusting for different sign conventions yields spin rotation values of

$$\frac{d\phi_{\text{PV}}^{np}}{dl} \approx 3 \times 10^{-7} \frac{\text{rad}}{\text{m}} . \quad (\text{VII.5})$$

for np spin rotation and

$$\frac{d\phi_{\text{PV}}^{nd}}{dl} \approx 5 \times 10^{-7} \frac{\text{rad}}{\text{m}} . \quad (\text{VII.6})$$

in the nd case. Note that there is a large spread in the DDH “reasonable ranges” surrounding these DDH “best estimates.”

We now compare our estimated result with the results from other calculations. Without measured PV parameters, none of these can be considered as more than order-of-magnitude estimates. Hence we do not normalize with respect to less than order-of-magnitude changes in choice of target density, for example.

Our estimate for the np spin rotation angle agrees well with earlier results obtained in the DDH and hybrid formalisms [13, 14, 16, 24], which found rotation angles between $5.15 \times 10^{-7} \frac{\text{rad}}{\text{m}}$ and $1.36 \times 10^{-6} \frac{\text{rad}}{\text{m}}$, depending on model choices made for the couplings and the strong interaction potentials.

The rotation angle in neutron deuteron spin rotation was determined in Ref. [15] using the DDH model and the Argonne v_{18} interaction, supplemented with the Urbana-IX three-nucleon potential. The result is

$$\frac{d\phi_{\text{PV}}^{nd}}{dl} = 9.32 \times 10^{-7} \frac{\text{rad}}{\text{m}} , \quad (\text{VII.7})$$

while a subsequent calculation also employing the $\text{Av}_{18} + \text{UIX}$ potentials found [17],

$$\frac{d\phi_{\text{PV}}^{nd}}{dl} = 7.68 \times 10^{-7} \frac{\text{rad}}{\text{m}} . \quad (\text{VII.8})$$

This agrees with our findings that the coefficients of the PV couplings in np and nd rotations are of the same order of magnitude, and also agrees with our rough estimate of Eq. (VII.4). Note that result (VII.8) is just one of several nd spin rotation predictions provided by Ref. [17], who consider two other parameter set estimations in addition to a set with the “best values” from the wide ranges provided by DDH. These two parameter sets, collected by Bowman [45], yield values of -6.82×10^{-7} and $-8.91 \times 10^{-7} \frac{\text{rad}}{\text{m}}$.

In addition, Refs. [15] and [17] performed a hybrid calculation in which the phenomenological wave functions of the PC sector are combined with a PV potential derived from $\text{EFT}(\pi)$. In this approach the consistency of treating interactions, wave functions, and currents within a unified framework is lost. In particular, different degrees of freedom appear in the PC and PV interactions. In both references, results for two different values of the regularization parameter μ used in the PV $\text{EFT}(\pi)$ potential are given, while in the PC sector a particular pionful potential with a fixed parameter set is used. For the choices $\mu = 138 \text{ MeV}$ and $\mu = 1 \text{ GeV}$, the results for the coefficients multiplying the PV parameters differ by up to two orders of magnitude. While this regularization dependence can in principle be removed by running the PV couplings to absorb cutoff dependence, these large differences are an indication of the resolution mismatch between $\text{EFT}(\pi)$ and the phenomenological potentials. Also note that different regularization schemes and degrees of freedom are employed for PC and PV interactions. Since the renormalization-scale dependence of the PV and PC couplings in the hybrid formalism is unknown, one cannot determine whether the calculation is indeed cutoff-independent, and varying the cutoff cannot be used to assess residual theoretical uncertainties. On the other hand, as shown above, our results are independent of any choices related to regularization and renormalization within the errors estimated in the EFT approach.

VIII. CONCLUSION AND OUTLOOK

At NLO in parity-violating $\text{EFT}(\pi)$, two- and three-body low-energy PV observables depend upon five unknown LECs, the $g^{(X-Y)}$ of Eq. (IV.1). PV $\text{EFT}(\pi)$ is based on the symmetries of QCD and the weak interaction, and the power counting of the theory. In order to verify that QCD is appropriately encoded into this EFT, it must be demonstrated that the LECs extracted from independent observables are consistent and are of “natural”

size $\sim \mathcal{O}(1)$ in dimensionless units. To overconstrain the system requires more than five model-independent calculations involving linearly independent combinations of the LECs, and the availability of the corresponding measurements.

This paper provides two of these calculations: Using EFT(π) consistently in both PV and PC sectors of the nucleon interactions, we obtain model-independent results for neutron spin rotation in hydrogen and deuterium targets. At NLO they are given by

$$\begin{aligned} \frac{1}{\rho} \frac{d\phi_{\text{PV}}^{np}}{dl} = & \left([4.5 \pm 0.5] (2g^{(3S_1-3P_1)} + g^{(3S_1-1P_1)}) \right. \\ & \left. - [18.5 \pm 1.9] (g_{(\Delta I=0)}^{(1S_0-3P_0)} - 2g_{(\Delta I=2)}^{(1S_0-3P_0)}) \right) \text{rad MeV}^{-\frac{1}{2}} \end{aligned}$$

for np , and

$$\begin{aligned} \frac{1}{\rho} \frac{d\phi_{\text{PV}}^{nd}}{dl} = & \left([8.0 \pm 0.8] g^{(3S_1-1P_1)} + [17.0 \pm 1.7] g^{(3S_1-3P_1)} \right. \\ & \left. + [2.3 \pm 0.5] (3g_{(\Delta I=0)}^{(1S_0-3P_0)} - 2g_{(\Delta I=1)}^{(1S_0-3P_0)}) \right) \text{rad MeV}^{-\frac{1}{2}} \end{aligned}$$

for nd . They yield two independent constraints on the five LECs. Absent any cancellation between different PV parameters we estimate that the rotation angles for both hydrogen and deuterium targets are of the same size,

$$\left| \frac{d\phi_{\text{PV}}}{dl} \right| \approx [10^{-7} \dots 10^{-6}] \frac{\text{rad}}{\text{m}} . \quad (\text{VIII.1})$$

There is no indication that the spin rotation observable is enhanced for a deuteron target, in agreement with Refs. [15, 17]. Numerical stability analyses verify the theoretical findings of Ref. [38] that no parity-violating 3NI is necessary at leading or next-to-leading order.

The two calculations presented here join three others published in the same framework; the longitudinal asymmetry in $\vec{p}p$ scattering [1] and two PV observables from the $np \leftrightarrow d\gamma$ system [2]. Note that other two-nucleon PV calculations using pionless EFT can be found in Refs. [24, 46, 47]. To go beyond consistency to the realm of potential prediction, we will next consider PV observables in Nd scattering, $nd \longleftrightarrow {}^3\text{H}\gamma$ and $pd \longleftrightarrow {}^3\text{He}\gamma$ before considering heavier systems.

Acknowledgments

While this paper was under review, J. Vanasse posted Ref. [26] with a result on spin rotation off deuterium. We thank him for discussions clarifying some differences between his and

our results that led to the correction of an error in our calculations. We thank D. R. Phillips for important suggestions and encouragement; M. Snow for extensive discussions on possible future PV experiments and his detailed write-up of spin-rotation definitions; as well as V. Gudkov, A. Micherdzinska, A. K. Opper, M. Paris, and Y. -H. Song for insightful discussions and helpful suggestions. We are particularly indebted to the organizers and participants of the Department of Energy's Institute for Nuclear Theory (INT) program 10-01: "Simulations and Symmetries" at the University of Washington, and for the Department of Energy's financial support of our visit. HWG is grateful for the kind hospitality of the Nuclear Experiment group of the Institut Laue-Langevin (Grenoble, France). MRS thanks the Lattice and Effective Field Theory group at Duke University for their hospitality. This work was carried out in part under National Science Foundation CAREER award PHY-0645498 (HWG, MRS), and US-Department of Energy grants DE-FG02-95ER-40907 (HWG, MRS) and DE-FG02-05ER41368 (RPS). We also acknowledge support by University Facilitating Funds of the George Washington University (HWG), and by the Center for Nuclear Studies of the George Washington University (HWG, MRS).

Appendix A: Partial-Wave Projectors

In this Appendix we construct the projectors used to extract the desired partial wave state(s) from a given $Nd_{s/t}$ state. The partial wave state is labelled $[^{2S+1}L_J, I]$, where S is the total spin, L the orbital angular momentum, J the total angular momentum, and I the isospin. The projectors given here do not exhaust what is needed to do a partial wave decomposition for higher order or inelastic calculations; that would require constructing projectors acting on NNN states as well. We employ the cluster-configuration basis introduced in Ref. [31], which also presents the S-wave projectors.

The $N^{a\alpha}$ field has two free indices: the SU(2) isospin index a and the SU(2) spin index α . The dibaryon field d_t^i is an isosinglet and spin-triplet (3S_1) with a free vector index i , while d_s^A is an isovector and spin-singlet (1S_0) with a free isovector index A . To obtain a total $S = \frac{1}{2}$ from an $Nd_{s/t}$ combination (indices suppressed), we can consider Nd_s , which is already purely $S = \frac{1}{2}$ from the SU(2) decomposition $\frac{1}{2} \otimes \mathbf{0} = \frac{1}{2}$. An $S = \frac{1}{2}$ term is also available from Nd_t via $\frac{1}{2} \otimes \mathbf{1} = \frac{3}{2} \oplus \frac{1}{2}$. The $S = \frac{1}{2}$ piece is isolated by contracting with a Pauli matrix in spin space: $\frac{1}{\sqrt{3}}(\sigma_i)^\mu_\alpha N^{a\alpha} d_t^i$. Summation of repeated indices is implied. The

normalization chosen will be explained at the end of this Section.

An $S = \frac{3}{2}$ term can only be obtained from Nd_t . It has four degrees of freedom in spin space: one free vector index (the i in d_t^i) with one free SU(2) spin index (the α in $N^{a\alpha}$) gives six degrees of freedom, but the two that contribute to $S = \frac{1}{2}$ are removed by additional constraints on the projector. The most general form is given by

$$Q^i_j = a\delta_j^i + b\sigma^i\sigma_j. \quad (\text{A.1})$$

Requiring that the $S = \frac{1}{2}$ and $S = \frac{3}{2}$ projectors are orthonormal

$$\sigma_i Q^i_j = 0 = Q^i_j \sigma^j, \quad Q^i_k Q^k_j = Q^i_j, \quad (\text{A.2})$$

yields

$$Q^i_j = \delta_j^i - \frac{1}{3}\sigma^i\sigma_j = \frac{1}{3}[2\delta_j^i - i\epsilon^i_{jk}\sigma^k], \quad (\text{A.3})$$

where the second expression uses $\sigma^i\sigma_j = \delta_j^i + i\epsilon^i_{jk}\sigma^k$. Orthogonality to the $S = \frac{1}{2}$ projector results in the required constraints that reduce the number of degrees of freedom to four.

The projector onto $S = \frac{3}{2}$ satisfies

$$(Q^i_j)^\dagger = Q^j_i. \quad (\text{A.4})$$

For P-waves, the projector is obtained by combining $L = 1$ powers of the unit vector \vec{e} in the direction of the $d_{s/t}$ center-of-mass momentum with the auxiliary field $d_{s/t}$ and the nucleon. In the case of the spin-1 field d_t , this leads to total angular momentum $\mathbf{1} \otimes \mathbf{1} \otimes \frac{1}{2} = \frac{5}{2} \oplus \frac{3}{2} \oplus \frac{1}{2}$. The projector onto $J = \frac{5}{2}$ is:

$$Q^{ij}_{kl} := \frac{9}{10} \left[(\delta_k^i \delta_l^j + \delta_l^i \delta_k^j - 2\delta^{ij} \delta_{kl}) - \frac{i}{3} (\epsilon^i_{km} \delta_l^j + \epsilon^j_{km} \delta_l^i + \epsilon^i_{lm} \delta_k^j + \epsilon^j_{lm} \delta_k^i) \sigma^m \right], \quad (\text{A.5})$$

which is symmetric and traceless in (ij) and (kl) separately,

$$\delta_{ij} Q^{ij}_{kl} = \delta^{kl} Q^{ij}_{kl} = 0, \quad Q^{ij}_{kl} = Q^{ji}_{kl}, \quad Q^{ij}_{kl} = Q^{ij}_{lk}, \quad (\text{A.6})$$

$$(Q^{ij}_{kl})^\dagger = Q^{kl}_{ij}, \quad (\text{A.7})$$

and orthonormal to the $S = \frac{1}{2}$ and $S = \frac{3}{2}$ projectors above:

$$\sigma_i Q^{ij}_{kl} = Q^{ij}_{kl} \sigma^k = 0, \quad Q^m_i Q^{ij}_{kl} = Q^{ij}_{kl} Q^l_m = 0, \quad Q^{ij}_{mn} Q^{mn}_{kl} = Q^{ij}_{kl}. \quad (\text{A.8})$$

Projectors onto definite states are obtained by contracting σ_j and Q^i_j with $d_{s/t}N$ to extract the desired spin-state and multiplying by L powers of momentum. Any remaining free

indices are then contracted with the appropriate projector onto the desired total angular momentum, which is again given by σ_j , Q^i_j , or Q^{ij}_{kl} , and with Kronecker-Deltas or ϵ^{ijk} as needed. For example, $(\sigma_k e^k)(\sigma_l d_t^l N)$ has the quantum numbers $S = \frac{1}{2}, J = \frac{1}{2}, L = 1$, i.e. ${}^2P_{\frac{1}{2}}$. Or, as a more complex example: ${}^4P_{\frac{3}{2}}$ mandates first coupling $d_t^l N$ to $S = \frac{3}{2}$ using Q^m_l , resulting in $Q^m_l d_t^l N$, and then multiplying by e_k . The two free vector indices have to be contracted with another projector Q^i_n , multiplied from the left, such that a $J = \frac{3}{2}$ state results. This can only be achieved by multiplying with ϵ^{nk}_m . The projector is thus proportional to $Q^i_n \epsilon^{nk}_m e_k Q^m_l d_t^l N$.

The same construction principle holds for isospin projections. States with $I = \frac{1}{2}$ can be generated by combining either d_t ($I = 0$) or d_s ($I = 1$) with the $I = \frac{1}{2}$ field N , since as before $\mathbf{0} \otimes \frac{1}{2} = \frac{1}{2}$ and $\mathbf{1} \otimes \frac{1}{2} = \frac{3}{2} \oplus \frac{1}{2}$. To obtain an $S = \frac{1}{2}, I = \frac{1}{2}$ state, first contract all spin-vector indices of $d_t^l N^{a\alpha}$ using σ_l , or all isospin-vector indices of $d_s^A N^{a\alpha}$ using τ_A , leading to two equivalent terms

$$[(\sigma_i)^\alpha_\beta \delta_b^a d_t^i + (\tau_A)^a_b \delta_\beta^\alpha d_s^A] N^{b\beta} \equiv [\sigma_i d_t^i + \tau_A d_s^A] N. \quad (\text{A.9})$$

Here, all spin and isospin indices are listed explicitly in the first expression, while obvious index contractions are suppressed in the second. As two cluster-configurations exist, namely $d_t N$ and $d_s N$, it is convenient to follow Ref. [48, App. A.1] in decomposing all operators as

$$\mathcal{O} = N_{b\beta}^\dagger \begin{pmatrix} d_{t,j}^\dagger & d_{s,B}^\dagger \end{pmatrix} \begin{pmatrix} \mathcal{O}(Nd_t \rightarrow Nd_t)_i^j & \mathcal{O}(Nd_s \rightarrow Nd_t)_A^j \\ \mathcal{O}(Nd_t \rightarrow Nd_s)_i^B & \mathcal{O}(Nd_s \rightarrow Nd_s)_A^B \end{pmatrix}_{a\alpha}^{b\beta} \begin{pmatrix} d_t^i \\ d_s^A \end{pmatrix} N^{a\alpha}. \quad (\text{A.10})$$

Each operator is represented in the cluster-configuration basis by a 2x2-matrix which carries spin and isospin indices, and all operators act in the direct tensor product space **spin** \otimes **isospin** \otimes **cluster**. The operator in the cluster-configuration basis that projects onto the $S = \frac{1}{2}, I = \frac{1}{2}$ component is

$$(\mathcal{P}_{d,iA})^{m\mu}_{a\alpha} = \frac{1}{\sqrt{3}} \begin{pmatrix} \sigma_i & 0 \\ 0 & \tau_A \end{pmatrix}_{a\alpha}^{m\mu}. \quad (\text{A.11})$$

On the other hand, only $d_t N$ contains an $S = \frac{3}{2}, I = \frac{1}{2}$ component, so that it is useful to define

$$(\mathcal{P}_{q,j}^i)^{m\mu}_{a\alpha} = \begin{pmatrix} Q^i_j & 0 \\ 0 & 0 \end{pmatrix}_{a\alpha}^{m\mu} = Q^i_j \mathcal{P}_q \quad \text{with } \mathcal{P}_q := \begin{pmatrix} 1 & 0 \\ 0 & 0 \end{pmatrix}. \quad (\text{A.12})$$

Here, \mathcal{P}_q is the matrix projecting onto the only physical component of the $S = \frac{3}{2}$ cluster-configuration matrix. The following relations hold:

$$\begin{aligned} \mathcal{P}_d^{iA} &= (\mathcal{P}_{d,iA})^\dagger = \text{“}\mathcal{P}_{d,iA}\text{”} , \quad \mathcal{P}_{d,iA} \mathcal{P}_d^{iA} = \mathbb{1} , \\ (\mathcal{P}_{q,i}^j)^\dagger &= \mathcal{P}_{q,j}^i , \quad \mathcal{P}_{q,j}^k \mathcal{P}_{q,i}^j = \mathcal{P}_{q,i}^k \mathcal{P}_{d,iA} \mathcal{P}_{q,j}^i = 0 . \end{aligned} \quad (\text{A.13})$$

The unit matrix in spin and isospin space is $(\mathbb{1})^{b\beta}_{a\alpha} = \delta_\alpha^\beta \delta_a^b$.

Below are the projectors as sources of the fields N and $d_{s/t}$ with the desired quantum numbers. First, in analogy with the auxiliary two-nucleon fields $d_{s/t}$, we introduce three-nucleon interpolating fields with the quantum numbers of the $Nd_{s/t}$ state. In symbolic notation, they are the cluster-configuration vectors representing sources $T^{[2S+1]L_J, I]^\dagger$ with total spin S , orbital angular momentum L , total angular momentum J , isospin I , and appropriate vector and spinor indices $\{M\}$. The projection onto a definite partial wave in cluster-configuration space is then

$$(T^{[2S+1]L_J, I]^\dagger)_{\{M\}} \mathcal{P}^{\{M\}}_{lA} [^{2S+1}L_J, I] \begin{pmatrix} d_t^l \\ d_s^A \end{pmatrix} N . \quad (\text{A.14})$$

The complete set of S- or P-wave projectors using auxiliary fields as source states is finally:

$$\begin{aligned} \mathcal{P}[^2S_{\frac{1}{2}}, I = \frac{1}{2}]_{lA} &= \mathcal{P}_{d,lA} , \\ \mathcal{P}[^2P_{\frac{1}{2}}, I = \frac{1}{2}]_{lA} &= (\vec{\sigma} \cdot \vec{e}) \mathcal{P}_{d,lA} , \\ \mathcal{P}[^2P_{\frac{3}{2}}, I = \frac{1}{2}]^i_{lA} &= \sqrt{3} Q^i_k e^k \mathcal{P}_{d,lA} , \\ \mathcal{P}[^4S_{\frac{3}{2}}, I = \frac{1}{2}]^i_l &= \mathcal{P}_{q,l}^i \equiv Q^i_l \mathcal{P}_q , \\ \mathcal{P}[^4P_{\frac{1}{2}}, I = \frac{1}{2}]_l &= \sqrt{\frac{3}{2}} e_k Q^k_l \mathcal{P}_q , \\ \mathcal{P}[^4P_{\frac{3}{2}}, I = \frac{1}{2}]^i_l &= \frac{3i}{\sqrt{5}} Q^i_n \epsilon^{nk}_m e_k Q^m_l \mathcal{P}_q = \frac{1}{3\sqrt{5}} [\sigma^i \delta_l^k + \sigma_l \delta^{ik} - 4\sigma^k \delta_l^i - 5i \epsilon^{ik}_l] e_k \mathcal{P}_q , \\ \mathcal{P}[^4P_{\frac{5}{2}}, I = \frac{1}{2}]^{ij}_l &= Q^{ij}_{kl} e^k \mathcal{P}_q . \end{aligned} \quad (\text{A.15})$$

The spin-quartet projectors carry no isovector index; the normalization is discussed below.

The two expressions for $\mathcal{P}[^4P_{\frac{3}{2}}]$ are equivalent since Q^m_l contains two Pauli matrices and is multiplied with one more from the left, and products of Pauli matrices can be reduced to a sum of terms containing at most one Pauli matrix. The first form contains the spin-quartet projector $\mathcal{P}_{q,l}^m \equiv Q^m_l \mathcal{P}_q$ explicitly and hence is manifestly orthogonal to the spin-

doublet projectors. The second form contains the minimal number of linearly independent structures, derived by building the most general matrix A^i_{kl} out of σ^i , δ^i_j and ϵ^{ijk} .

The orthonormalization condition was imposed as follows: Projectors to different partial waves are orthogonal after contraction over the auxiliary-field variable (lA) and integration over the solid angle element $d\Omega_e$ of the auxiliary field cm-momentum direction \vec{e} :

$$\frac{1}{4\pi} \int d\Omega_e \mathcal{P}^{[2S+1]L_J, I] \{M\}_{lA}} \left(\mathcal{P}^{[2S'+1]L'_{J'}, I']^\dagger \right)^{lA}_{\{N\}} = 0 \quad \forall \quad L \neq L' \vee S \neq S' \vee J \neq J' \vee I \neq I'. \quad (\text{A.16})$$

When the states are identical, integration and contraction must yield the identity element in the space of total angular momentum states. In the cluster-configuration basis notation:

$$\text{for } J = \frac{1}{2}: \quad \frac{1}{4\pi} \int d\Omega_e \mathcal{P}^{[2S+1]L_{\frac{1}{2}}, I]_{lA}} \mathcal{P}^\dagger^{[2S+1]L_{\frac{1}{2}}, I]^{lA}} = \mathbb{1}, \quad (\text{A.17})$$

$$\text{for } J = \frac{3}{2}: \quad \frac{1}{4\pi} \int d\Omega_e \mathcal{P}^{[2S+1]L_{\frac{3}{2}}, I]^i_{lA}} \mathcal{P}^\dagger^{[2S+1]L_{\frac{3}{2}}, I]^{lA}_j} = \begin{cases} Q^i_j & \text{for } S = \frac{1}{2}, \\ Q^i_j \mathcal{P}_q & \text{for } S = \frac{3}{2}, \end{cases} \quad (\text{A.18})$$

$$\text{for } J = \frac{5}{2}: \quad \frac{1}{4\pi} \int d\Omega_e \mathcal{P}^{[2S+1]L_{\frac{5}{2}}, I]^{ij}_{mn}} \mathcal{P}^\dagger^{[2S+1]L_{\frac{5}{2}}, I]^{mn}_{kl}} = Q^{ij}_{kl} \mathcal{P}_q. \quad (\text{A.19})$$

Appendix B: Assessing choices for the PC amplitudes of the class-II diagrams

In this Appendix, we discuss in more detail the choices of the PC amplitudes $t[X; k, q]$ of Eq. (VI.13) in the class-II contributions at NLO appearing in Eqs. (VI.10/VI.11/VI.12) and shown in Fig. 11. As discussed in the main text, the convolution kernel itself is already NLO, so that in principle a LO PC amplitude suffices. Figures 15, 16 and 17 compare the dependence of the total amplitudes on the different treatments of $t[X; k, q]$, benchmarked against the leading-order result and the choice of Eq. (VI.13) to include the $^{2,4}\text{S}$ -wave amplitudes as NLO and the $^{2,4}\text{P}$ -wave amplitudes as LO, see Eq. (VI.13).

Consider first the inclusion of the PC $^2\text{S}_{\frac{1}{2}}$ -wave amplitude at LO instead of NLO (+ in Fig. 15), while treating all other amplitudes according to Eq. (VI.13). This leads to individual contributions diverging logarithmically and as $q^{0.23\dots}$, as demonstrated on general grounds in Ref. [38] and numerically confirmed here. The problem is evident in the Λ dependence of the functions d and c of Eqs. (VI.19) and (VI.25), as shown in Figs. 15 and 17. This choice must thus be discarded as not properly renormalized.

Next, it is consistent to include the PC $^4\text{S}_{\frac{3}{2}}$ -wave amplitude at LO instead of NLO (\times in

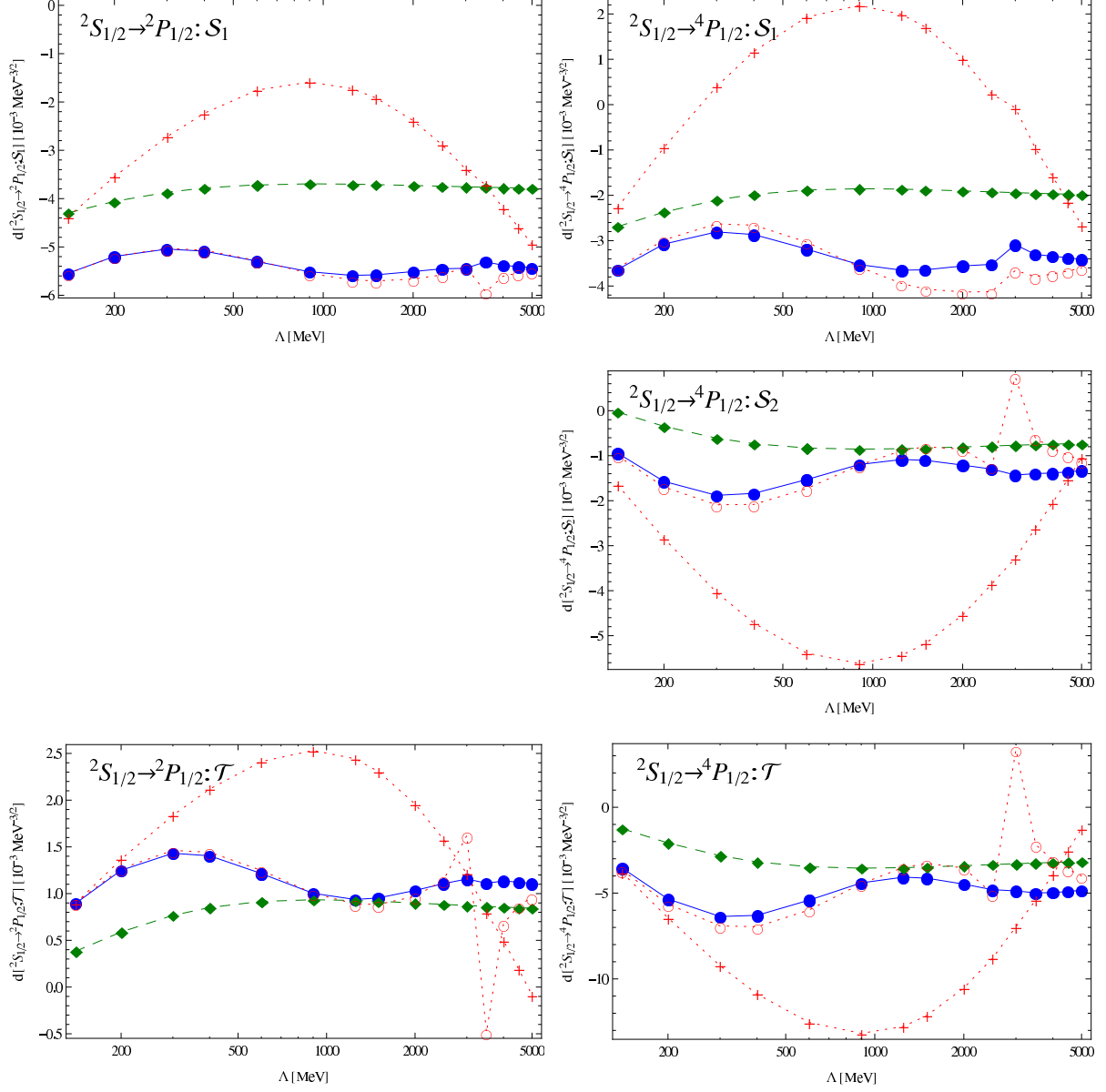


Figure 15: Cutoff dependence of the functions $d[{}^2S_{1/2} \rightarrow Y; \text{coupling}]$, Eq. (VI.19), for different choices of the order of the PC amplitudes in the class-II contributions of Fig. 11 and Eqs. (VI.10/VI.11/VI.12). \blacklozenge (dashed lines): LO result, 3NI H_0 from nd ${}^2S_{1/2}$ -scatt. length; all other: NLO results with different treatments of PC amplitudes, with 3NI from ${}^2S_{1/2}$ -scatt. length. \bullet (solid lines): PC amplitudes ${}^2S_{1/2}$ as NLO, ${}^{2,4}P$ as LO (Eq. (VI.13)); \circ (dotted lines): all as NLO; $+$ (dotted lines): all as LO. Linear extrapolations used to guide the eye. Notice the different scales on the vertical axes. Amplitudes which are identically zero are not displayed. Columns (left to right): partial waves ${}^2S_{1/2} \rightarrow {}^2P_{1/2}$, ${}^2S_{1/2} \rightarrow {}^4P_{1/2}$; rows (top to bottom): coefficients of \mathcal{S}_1 , \mathcal{S}_2 , \mathcal{T} .

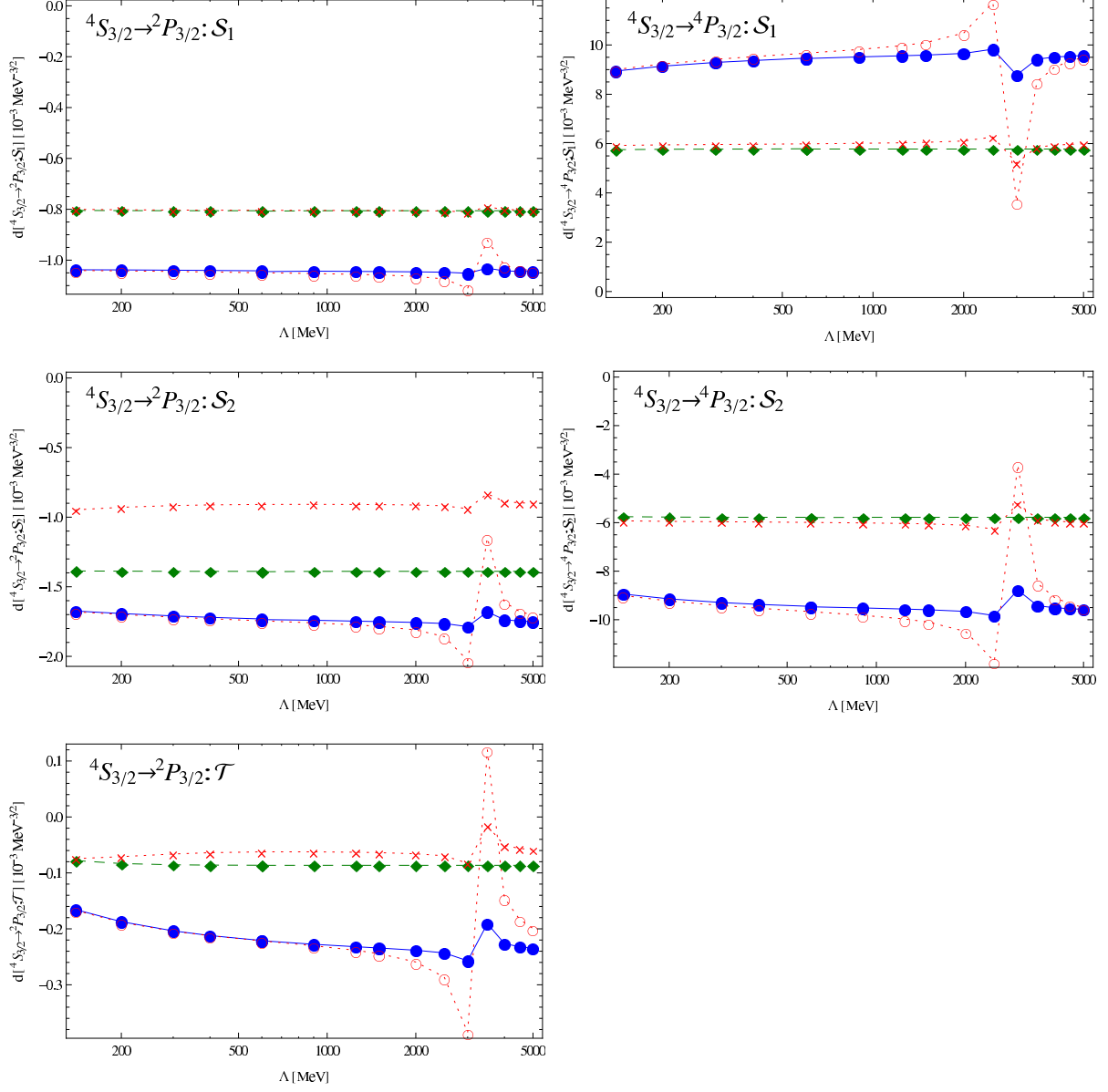


Figure 16: Cutoff dependence of the expansion coefficients $d[{}^4S_{\frac{3}{2}} \rightarrow Y; \text{coupling}]$, Eq. (VI.19), for different choices of the order of the PC amplitudes in the class-II contributions of Fig. 11 and Eqs. (VI.10/VI.11/VI.12). \blacklozenge (dashed lines): LO result; all other: NLO results with different treatments of PC amplitudes. \bullet (solid lines): PC amplitudes ${}^4S_{\frac{3}{2}}$ as NLO, ${}^2,{}^4P$ as LO (Eq. (VI.13)); \circ (dotted lines): all as NLO; \times (dotted lines): all as LO. Linear extrapolations used to guide the eye. Notice the different scales on the vertical axes. Amplitudes which are identically zero are not displayed. Columns (left to right): partial waves ${}^4S_{\frac{3}{2}} \rightarrow {}^2P_{\frac{3}{2}}$, ${}^4S_{\frac{3}{2}} \rightarrow {}^4P_{\frac{3}{2}}$; rows (top to bottom): coefficients of \mathcal{S}_1 , \mathcal{S}_2 , \mathcal{T} .

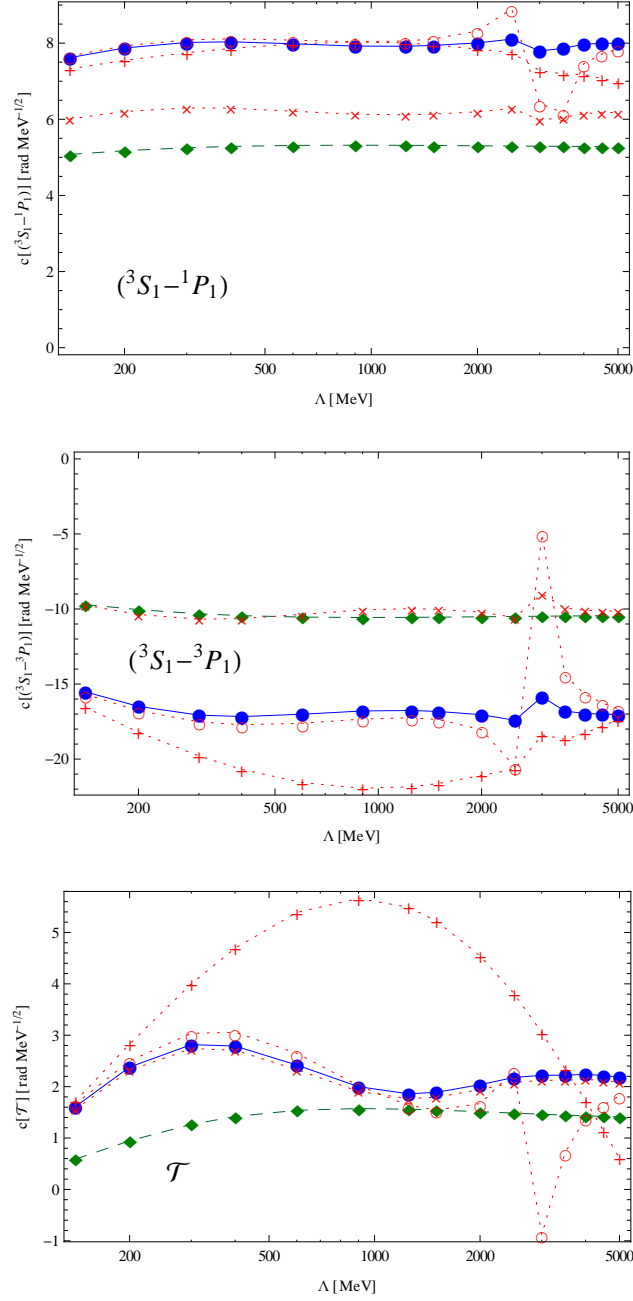


Figure 17: Cutoff dependence of the expansion coefficients $c[g^{(X-Y)}]$ of the neutron spin-rotation angle in deuterium, Eq. (VI.25), for different choices of the order of the PC amplitudes in the class-II contributions of Fig. 11 and Eqs. (VI.10/VI.11/VI.12). Notation as in Figs. 15 and 16. Linear extrapolations to guide the eye; different scales on the vertical axes.

Fig. 16), while treating all other amplitudes according to Eq. (VI.13). This still determines the PV amplitudes at NLO since the kernel of the convolution already counts as NLO. With the exception of $d[{}^4S_{\frac{3}{2}} \rightarrow {}^2P_{\frac{3}{2}}, \mathcal{S}_2]$, however, the corresponding results are very close to those obtained in a LO calculation of the PV amplitudes (\blacklozenge). Using the PC ${}^4S_{\frac{3}{2}}$ -wave amplitude at NLO (\bullet and \circ) induces a considerable shift of all functions $d[{}^4S_{\frac{3}{2}} \rightarrow Y; \text{coupling}]$. As discussed in Sec. VIB, PC LO and NLO ${}^4S_{\frac{3}{2}}$ amplitudes predict values of the ${}^4S_{\frac{3}{2}}$ scattering length that differ by about 25%, with the NLO result very close to the experimental value. The PV amplitudes, and therefore the $d[{}^4S_{\frac{3}{2}} \rightarrow Y; \text{coupling}]$, are expected to be highly sensitive to the ${}^4S_{\frac{3}{2}}$ scattering length. This is supported by the plots in Fig. 16. We therefore choose the NLO amplitude for the PC ${}^4S_{\frac{3}{2}}$ wave. Higher-order corrections from the ${}^4S_{\frac{3}{2}}$ -wave amplitude are expected to be small, since the NLO expression for the scattering length is already in good agreement with experiment.

Finally, it is consistent to include the PC ${}^{2,4}P$ -wave amplitudes at NLO (\circ in Figures) instead of LO (\bullet in Figures), while treating all other amplitudes according to Eq. (VI.13). One might speculate that this leads to significant changes since the zero-energy effective-range parameter of the amplitudes, the scattering volume, is up to a factor of 2 bigger at NLO than at LO; see Ref. [31]. Instead, the amplitudes appear largely insensitive to the effective-range parameters of the P-waves. However, the spurious cutoff dependence already seen when the P-wave amplitudes are included at LO is widened and increased to a pole in the window $\Lambda \in [2000 \dots 4000]$ MeV in the total amplitudes. Its origin seems to be that the partially-resummed approach includes some contributions beyond NLO which need to be renormalized by ${}^{2,4}P$ -wave 3NIs which are not present at NLO. Outside that window, the functions c and d agree with the choice made in Eq. (VI.13) within the error-estimate of Sec. VIE.

-
- [1] D. R. Phillips, M. R. Schindler, R. P. Springer, Nucl. Phys. **A822**, 1-19 (2009). [arXiv:0812.2073 [nucl-th]].
 - [2] M. R. Schindler, R. P. Springer, Nucl. Phys. **A846**, 51-62 (2010). [arXiv:0907.5358 [nucl-th]].
 - [3] E. G. Adelberger, W. C. Haxton, Ann. Rev. Nucl. Part. Sci. **35**, 501-558 (1985).
 - [4] M. J. Ramsey-Musolf, S. A. Page, Ann. Rev. Nucl. Part. Sci. **56**, 1-52 (2006).

- [hep-ph/0601127].
- [5] F. C. Michel, Phys. Rev. **133**, B329-B349 (1964).
 - [6] L. Stodolsky, Phys. Lett. **B50**, 352 (1974).
 - [7] L. Stodolsky, Phys. Lett. **B96**, 127 (1980).
 - [8] L. Stodolsky, Nucl. Phys. **B197**, 213 (1982).
 - [9] W. M. Snow, C. D. Bass, T. D. Bass, B. E. Crawford, K. Gan, B. R. Heckel, D. Luo, D. M. Markoff *et al.*, Phys. Rev. **C83**, 022501 (2011).
 - [10] G. S. Danilov, Phys. Lett. **18**, 40 (1965); Phys. Lett. **B35**, 579 (1971). Sov. J. Nucl. Phys. **14**, 443 (1972).
 - [11] B. Desplanques, J. F. Donoghue, B. R. Holstein, Annals Phys. **124**, 449 (1980).
 - [12] V. F. Dmitriev, V. V. Flambaum, O. P. Sushkov, V. B. Telitsin, Phys. Lett. **B125**, 1-4 (1983).
 - [13] Y. Avishai, P. Grange, J. Phys. G **G10**, L263-L270 (1984).
 - [14] R. Schiavilla, J. Carlson, M. W. Paris, Phys. Rev. **C70**, 044007 (2004). [nucl-th/0404082].
 - [15] R. Schiavilla, M. Viviani, L. Girlanda, A. Kievsky and L. E. Marcucci, Phys. Rev. C **78**, 014002 (2008) [Erratum-ibid. C **83**, 029902 (2011)] [arXiv:0805.3599 [nucl-th]].
 - [16] C. -P. Liu, Phys. Rev. **C75**, 065501 (2007). [nucl-th/0609078].
 - [17] Y. -H. Song, R. Lazauskas, V. Gudkov, Phys. Rev. **C83**, 015501 (2011). [arXiv:1011.2221 [nucl-th]].
 - [18] S. R. Beane, P. F. Bedaque, W. C. Haxton, D. R. Phillips, M. J. Savage, In Shifman, M. (ed.): At the frontier of particle physics, vol. 1, 133-269. [nucl-th/0008064].
 - [19] P. F. Bedaque, U. van Kolck, Ann. Rev. Nucl. Part. Sci. **52**, 339-396 (2002). [nucl-th/0203055].
 - [20] L. Platter, Few Body Syst. **46**, 139-171 (2009). [arXiv:0904.2227 [nucl-th]].
 - [21] D. B. Kaplan, M. J. Savage, Nucl. Phys. **A556**, 653-671 (1993).
 - [22] M. J. Savage, R. P. Springer, Nucl. Phys. **A644**, 235-244 (1998). [nucl-th/9807014].
 - [23] D. B. Kaplan, M. J. Savage, R. P. Springer, M. B. Wise, Phys. Lett. **B449**, 1-5 (1999). [nucl-th/9807081].
 - [24] S. -L. Zhu, C. M. Maekawa, B. R. Holstein, M. J. Ramsey-Musolf, Uvan Kolck, Nucl. Phys. **A748**, 435-498 (2005). [nucl-th/0407087].
 - [25] J. Wasem, [arXiv:1108.1151 [hep-lat]].
 - [26] J. Vanasse, arXiv:1110.1039 [nucl-th].
 - [27] E. Fermi, Nuclear Physics, revised edition, University Of Chicago Press, Chicago, 1974.

- [28] D. B. Kaplan, Nucl. Phys. **B494**, 471-484 (1997). [nucl-th/9610052].
- [29] P. F. Bedaque, H. W. Griesshammer, Nucl. Phys. **A671**, 357-379 (2000). [nucl-th/9907077].
- [30] S. R. Beane, M. J. Savage, Nucl. Phys. **A694**, 511-524 (2001). [nucl-th/0011067].
- [31] H. W. Griesshammer, Nucl. Phys. **A744**, 192-226 (2004). [nucl-th/0404073].
- [32] D. B. Kaplan, M. J. Savage, M. B. Wise, Phys. Rev. **C59**, 617-629 (1999). [nucl-th/9804032].
- [33] D. R. Phillips, G. Rupak, M. J. Savage, Phys. Lett. **B473**, 209-218 (2000). [nucl-th/9908054].
- [34] I. S. Gradshteyn and I. M. Ryzhik, Table of Integrals, Series and Products, 5th edition, Academic Press, San Diego, 1994.
- [35] P. F. Bedaque, G. Rupak, H. W. Griesshammer, H. -W. Hammer, Nucl. Phys. **A714**, 589-610 (2003). [nucl-th/0207034].
- [36] W. Dilg, L. Koester, W. Nistler, Phys. Lett. B **36**, 208-210 (1971).
- [37] L. Girlanda, Phys. Rev. **C77**, 067001 (2008). [arXiv:0804.0772 [nucl-th]].
- [38] H. W. Griesshammer, M. R. Schindler, Eur. Phys. J. **A46**, 73-83 (2010). [arXiv:1007.0734 [nucl-th]].
- [39] M. L. Goldberger, K. M. Watson, Collision Theory; John Wiley & Sons, New York, 1964.
- [40] J. H. Hetherington, L. H. Schick, Phys. Rev. **137**, B935-B948 (1965); R. T. Cahill, I. H. Sloan, Nucl. Phys. **A165**, 161-179 (1971); R. Aaron, R. D. Amado, Phys. Rev. **150**, 857-866 (1966); E. W. Schmid, H. Ziegelmann, The Quantum Mechanical Three-Body Problem, Vieweg Tracts in Pure and Applied Physics Vol. 2, Pergamon Press (1974).
- [41] H. W. Hammer, T. Mehen, Phys. Lett. **B516**, 353-361 (2001). [nucl-th/0105072].
- [42] C. Ji, D. R. Phillips, L. Platter, [arXiv:1106.3837 [nucl-th]].
- [43] J. Kirscher, H. W. Griesshammer, D. Shukla, H. M. Hofmann, Eur. Phys. J. **A44**, 239-256 (2010). [arXiv:0903.5538 [nucl-th]].
- [44] P. D. Eversheim, W. Schmitt, S. E. Kuhn, F. Hinterberger, P. von Rossen, J. Chlebek, R. Gebel and U. Lahr *et al.*, Phys. Lett. B **256**, 11 (1991).
- [45] J. D. Bowman, “Hadronic Weak Interaction”, INT Workshop on Electric Dipole Moments and CP Violations, March 19-23, 2007, http://www.int.washington.edu/talks/WorkShops/int_07_1/.
- [46] M. J. Savage, Nucl. Phys. **A695**, 365-373 (2001). [nucl-th/0012043].
- [47] J. W. Shin, S. Ando, C. H. Hyun, Phys. Rev. **C81**, 055501 (2010). [arXiv:0907.3995 [nucl-th]].
- [48] H. W. Griesshammer, Nucl. Phys. **A760**, 110-138 (2005). [nucl-th/0502039].